Oct 2014

GLM - General Lake Model

Model Overview and User Information

v 2.0 β - Oct 2014

M.R. Hipsey, L.C. Bruce & D.P. Hamilton

The University of Western Australia

AED Aquatic Eco Dynamics

The University of Waikato
Te Whare Wānanga o Waikato

GLEON

Summary

The *General Lake Model* (GLM) is an open-access model developed for simulating lake dynamics. It simulates vertical stratification and mixing and accounts for the effect of inflows/outflows, surface heating and cooling, and it can be extended to include the effect of ice cover. GLM has been designed to be an open-source community model developed in collaboration with members of *Global Lake Ecological Observatory Network* (GLEON) to integrate with lake sensor data.

It is suited to environmental modelling studies where simulation of lakes or reservoirs is required. The one-dimensional (1D) basis of the model means it is suited to seasonal and decadal scale investigations of water quality but it can also be used in comparisons of simulation output against high-frequency sensor data. Sites that may be simulated with the model include deep and shallow lakes, drinking water, hydropower or irrigation reservoirs, mining pit lakes, wastewater ponds and urban wetlands. The model couples with the *Aquatic EcoDynamics* library (AED) for integrated simulations of lake and reservoir water quality and ecosystem health.

This manual summarises the scientific basis and numerical implementation of the model algorithms including the sub-models related to surface heat exchange and ice-cover dynamics, vertical mixing and the inflow/outflow dynamics. A summary of typical parameter values for lakes and reservoirs collated from a range of sources is included. The final section provides an overview of setting up and running the model. Further information for analysis of model outputs and undertaking sensitivity and uncertainty assessments with the model is also provided.

Acknowledgements

GLM has been developed by the Aquatic EcoDynamics Research Group team at UWA (http://aed.see.uwa.edu.au) in collaboration with the Lake Ecosystem Restoration research group at the University of Waikato (http://www.lernz.com). Funding for the initial development of the model was from the U.S. NSF Cyber-enabled Discovery and Innovation (CDI) grant awarded to Prof. Paul Hanson (lead investigator) and colleagues from 2009-2014. In addition to the named authors who have driven the scientific direction of the model, we acknowledge the software engineering of the model undertaken by Casper Boon at UWA. We also acknowledge numerous members of the GLEON ecosystem modelling working group and the associated multi-lake comparison project (MLCP), and in particular are grateful to Jordan Read and Luke Winslow form the USGS for extensive help. Through application of the model within the GLEON community we have been able to undertake extensive review of model performance on earlier versions and gain essential feedback on model features and operation. We also acknowledge development of the Bird Clear Sky Model for use within GLM by Aditya Singh from UWA.

Whilst GLM is a new code, it is based on the large body of historical research and publications produced by the Centre for Water Research at the University of Western Australia, which we acknowledge for the inspiration and guidance on the approach that has been adopted herein . We also acknowledge the MCMC code by Marko Laine that has been integrated with this GLM version model sensitivity and uncertainty assessment, (accessed from http://helios.fmi.fi/~lainema/mcmc/). Provision of the environmental symbols used for the GLM scientific diagrams are courtesy of the Integration and Application Network, University of Maryland Center for Environmental Science.

Citing this manual:
Hipsey, M.R., Bruce, L.C., Hamilton, D.P., 2014. GLM - General Lake Model: Model overview and user information. AED Report #26, The University of Western Australia, Perth, Australia. 42pp.

Copyright © 2014. The University of Western Australia.
ISBN: 978-1-74052-303-5

Contents

Overview

Background

The *General Lake Model* (GLM) is a one-dimensional hydrodynamic model for simulating the water balance and vertical stratification of lakes and other standing (lentic) water bodies. GLM computes vertical profiles of temperature, salinity and density by accounting for the effect of inflows and outflows on the water balance, in addition to surface heating and cooling, and vertical mixing (Figure 1). The model also includes the effects of ice cover formation and subsequent melting on the heating and mixing processes within the lake (Yao *et al*., 2014).

Since the model is one-dimensional it assumes no horizontal variability within the domain and users must therefore ensure their application of the model is suited to this assumption. For deep, stratified, systems, the model is ideally suited to long-term investigations ranging from months to decades, and for coupling with biogeochemical models to explore the role that stratification and vertical mixing play on lake ecosystem dynamics. However, the model can also be used, with some caution and checks, for shallow lakes, ponds or wetlands where the water column is relatively well mixed. A recent application of the model demonstrates its ability for including lakes in regional climate and earth system assessments (Read *et al*., 2014).

The model was initially built as a project within the *Global Lake Ecological Observatory Network* (GLEON) to provide a computationally efficient lake modelling platform to be used for integration with lake observatory systems and for training lake scientists. The model couples with the *Framework for Aquatic Biogeochemical Models* (FABM), and in particular is designed to operate with the *Aquatic EcoDynamics* modules (Hipsey, 2014) included within FABM (termed FABM-AED). Since its original development, the model has also been used successfully for simulating reservoirs, mining pit lakes and wetlands. The model is available freely and distributed as open-source under the GNU GPL license, and it is encouraged that the tool be adapted for a wide variety of applications so that we can advance lake simulation (Mooij *et al*., 2010; Trolle *et al*., 2012).

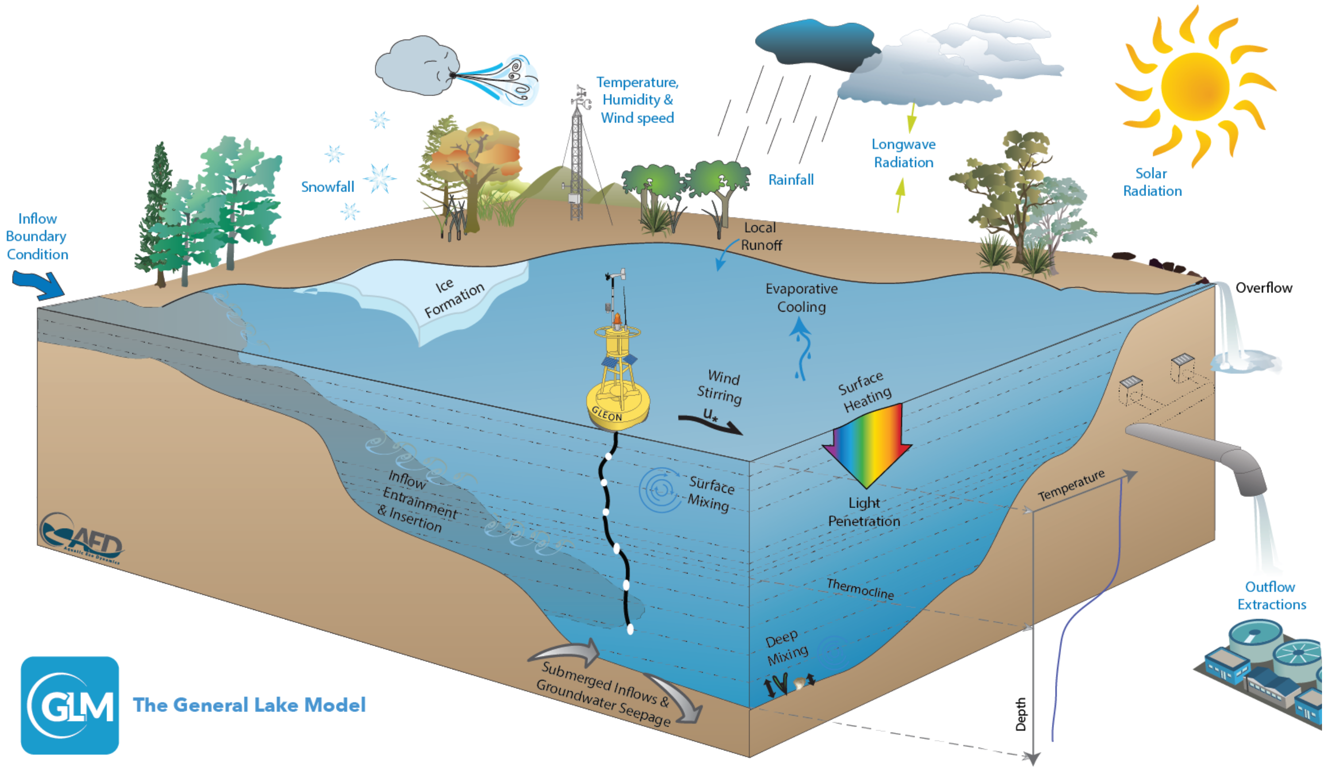

Figure 1: Schematic of a GLM simulation domain, input information (blue text) and key simulated processes (black text).

Model Approach

For background information of on the mixing dynamics of lakes readers are referred to summaries by Imboden and Wüest (1995) and Imberger and Patterson (1990). GLM adopts a one-dimension solution processes of vertical mixing by incorporating a series of vertical layers that are used to describe the variation in water column properties. The model adopts a flexible Lagrangian structure originally introduced for the model DYRESM by Imberger et al. (1978) and Imberger & Patterson (1981). Numerous model variations have since been introduced to further extend this conceptual approach through applications to a variety of lake and reservoir environments (e.g., Hocking & Patterson, 1991; Hamilton & Schladow 1997; McCord & Schladow, 1998; Gal et al., 2003; Yeates et al., 2004). The Lagrangian design assumes each layer is a 'control volume' that can change thickness by contracting and expanding in response to inflows, outflows, mixing with adjacent layers, and surface mass fluxes. Layers each have a unique density computed based on the local salinity and temperature and when sufficient energy becomes available to over come density differences between the adjacent layers, they will merge thus accounting for the process of mixing. For deeper systems, a stable vertical density gradient will form in response to periods of high solar radiation creating warm, less-dense conditions near the surface with cooler conditions deeper in the water separated by a thermocline region (metalimnion). Layer thicknesses are adjusted throughout the water column by the model in order to sufficiently resolve the vertical density gradient with fine resolution occurring in the thermocline and thicker cells where mixing is occurring (as depicted schematically in Figure 1). Unlike the fixed grid (Eulerian) design of most lake and ocean models, where mixing algorithms are typically based on resolving vertical velocities, it has been reported that numerical diffusion of the thermocline in this approach is limited, making it particularly suited to long-term investigations, and requiring limited site-specific calibration (Patterson et al., 1984; Hamilton & Schladow, 1997).

Although GLM is a new model code written in C, the core layer structure and mixing algorithms have been based on equations summarised in Hamilton and Schladow (1997) and Imberger and Patterson (1981), thereby making it similar to these previously reported models. Beyond this functionality, the model features numerous customisations and extensions in order to make it a fast and easy to use package suitable for a wide range of contemporary applications.

Model Suitability & Data Requirements

The model may be suitable for investigations where resolving the horizontal variability is not a requirement of the study. This includes natural lakes, large and small drinking water reservoirs and mining pit lakes. Despite the 1D assumption, the model performs well in reservoirs with dendritic morphometry (e.g., drowned river valleys) or more regular shapes. Whilst the model is able to resolve vertical stratification, it may be used to simulate shallow lakes, wetlands, wastewater ponds that experience well-mixed conditions. In this case, the layer structure will automatically simplify, and mass and energy will continue to be conserved. The model is suitable for operation in a wide range of climate conditions and is able to simulate ice formation, and also accommodate a range of atmospheric conditions.

Beyond modelling the water and heat balance of a lake, the model is well-suited to simulate water quality investigations through coupling with a water quality model library. The model is distributed pre-compiled with the AED WQ modelling libraries, and these are able to simulate turbidity, oxygen, nutrients, phytoplankton, zooplankton, pathogens and chemical variables.

In general, the model can be simplified to essential a body of water with minimal complexity. Users may configure any number of inflows and outflows and more advanced options exist for simulating the water and heat balance. At a minimum, the model requires the user to supply a hypsographic curve, $A = A(h)$, to describe the storage, elevation, and area relationships. Depending on the context of the simulation, either daily our hourly meteorological time-series data for surface forcing is required, and daily time-series of volumetric inflow and outflow rates may also be required. A summary of relevant parameters within the model and their default values are given in Tables at the end of the model science overview section.

The model may be run without any 3rd party software as the input files consist of "namelist" text files for configuration and csv files for meteorological and flow data. Further details of the model setup and file formats are outlined in the GLM Setup section.

Model Science Overview

Layer structure

The model is composed of a series of layers numbered from the lake bottom to the surface. The number of layers, $N_{LEV}(t)$, is adjusted throughout the simulation to maintain the assumption that each layer must have homogenous properties across the layer. Initially, the layers are assumed to be of equal thickness, and the initial number of layers, $N_{LEV}(t=0)$, depends on the user-defined minimum (h_{min}) and maximum (h_{max}) layer thickness limits that are set, and the lake depth (both defined in `glm.nml`, see model setup section). As the model simulation progresses, density changes due to surface heating, vertical mixing, and inflows and outflows lead to dynamic changes in the layer structure as layers expand or contract. The model includes routines to enforce the layer limits, maintaining the optimal thickness of layers required to resolve the vertical density gradient.

The layer volumes are determined by interpolating layer area off the user-specified hypsographic curve for the lake basin, such that $A_i = f(h_i)$, where i is the layer number. The user provides N_{BSN} depth points with basin area to define the hypsographic curve. Layers are generally at a relatively coarse resolution relative to the simulated layers, and the model can either i) accept prescribed volume values at each, or ii) compute the volumes assuming a simple interpolation. In the latter case, the first layer, V_1, is computed assuming a conical shape, and above that each point as:

$$V_b = V_{b-1} + [A_{b-1} + 0.5(A_b - A_{b-1})](h_b - h_{b-1}) \tag{1}$$

where $1 < b \leq N_{BSN}$. Using the raw hyposgraphic data, a refined depth-area-volume relationship is calculated during the simulation using finer depth increments (e.g., ~ 0.1 m), giving N_{MORPH} levels that are used for subsequent calculations. The area and volume at the depth of each increment, h_z is interpolated from the supplied information as:

$$V_z = V_{b-1}\left(\frac{h_z}{h_{b-1}}\right)^{\alpha_b} \quad \text{and} \quad A_z = A_{b-1}\left(\frac{h_z}{h_{b-1}}\right)^{\beta_b} \tag{2}$$

where V_z and A_z are the volume and area at each of the refined elevations of the refined depth vector, and V_z in these expressions refers to the nearest b level below h_z such that $h_{b-1} < h_z$. Note the interpolation coefficients are computed as:

$$\alpha_b = \left[\frac{log_{10}\left(\frac{V_{b+1}}{V_b}\right)}{log_{10}\left(\frac{h_{b+1}}{h_b}\right)}\right] \quad \text{and} \quad \beta_b = \left[\frac{log_{10}\left(\frac{A_{b+1}}{A_b}\right)}{log_{10}\left(\frac{h_{b+1}}{h_b}\right)}\right] \tag{3}$$

The density in each layer is computed based on the temperature, T, and salinity, S, at any given time according to the UNESCO (1981) equation of state: $\rho_i = \rho(T_i, S_i)$.

Water balance

The model solves the water balance of the lake domain by including several user-configurable fluxes. A daily summary of the water balance is provided to the user via the summary information in `lake.csv`. The main water balance components include:

- Surface mass fluxes
  - Evaporation
  - Rainfall
  - Snowfall
- Inflows
  - Surface inflows
  - Deep inflows
  - Runoff from the surrounding catchment
- Outflows
  - Withdrawals
  - Overflow
  - Seepage

The mass balance occurs through the layers, but evaporation and precipitation only occur in the surface layer and seepage only occurs form the bottom layer. The model computes the dynamics of the inflows and outflows on a daily time-step, however the surface mass fluxes can occur hourly or daily depending on the resolution of meteorological forcing data.

The change in surface layer thickness due to surface mass fluxes is summarised as:

$$\frac{dh_S}{dt} = E + S + f_R R + Q_R / A_s \tag{4}$$

where h_S is the height of the surface layer (m), t time step (s), E is the evaporation mass flux computed from the heat flux ϕ_E (W m^{-2}) described below, R is rainfall and S is snowfall (m day^{-1}), and f_R is a user-definable scaling factor that may be applied to increase or reduce the rainfall data (default = 1). Q_R is an optional term to account or runoff to the lake form the exposed banks, which may be important in reservoirs with a large drawdown range, or wetlands where periodic drying of the lake may occur. This calculated using a simple runoff model when the rainfall intensity exceeds the threshold, R_L (m day^{-1}):

$$Q_R = f_{ro}(f_R R - R_L)(A_{max} - A_s) \tag{5}$$

where f_{ro} is the runoff coefficient, defined as the fraction of rainfall that is converted to runoff to the lake's edge, and ius the maximum possible area of inundation of the lake (as defined by the area provided by the user at N_{BSN} area value).

Note that Eq 4 does not include changes to h_S as a result of mixing dynamics (i.e. the merging or splitting of layers ot enfoce the layer thickness limits), or ice formation/melt, or river inflows; these are described in subsequent sections. However, all layers within the domain also are subject to mass conservation and impacted by inflowing and outflowing water.

Surface energy budget

A balance of shortwave and long wave radiation fluxes, sensible and evaporative heat fluxes determine the net cooling and heating for GLM. The general heat budget equations can be described as:

$$\left[\frac{c_p}{A_s z_{sml}}\right]\frac{dT_S}{dt} = \phi_{SW_S} - \phi_E + \phi_H + \phi_{LWin} - \phi_{LWout} \tag{6}$$

where c_p is the specific heat capacity of air (1005 J/kg/°C), T_S is the surface temperature of the surface mixed layer and the RHS heat flux terms are expanded upon individually below. Several options exist for customizing the individual surface heat flux components and also summarised below.

Solar heating and light penetration

Solar radiation is the key driver of the lake thermodynamics, however, data may not always be available from a nearby pyranometer. GLM v2 users may choose to either have GLM compute surface irradiance from a theoretical approximation based on the Bird Clear Sky insolation model (Bird, 1984), modified for cloud cover, or alternatively hourly or daily solar radiation intensity data may be directly specified. If the former, then $\hat{\phi}_{SW}$ is calculated from (Bird, 1984; Luo *et al.*, 2010):

$$\hat{\phi}_{SW} = \frac{\hat{\phi}_{DB} + \hat{\phi}_{AS}}{1 - (\alpha_{SW}\ \alpha_{SKY})} f(C) \tag{7}$$

where the model computes total irradiance, $\hat{\phi}_{SW}$ (W m^{-2}), from direct beam $\hat{\phi}_{DB}$, and the irradiance from atmospheric scattering $\hat{\phi}_{AS}$ (refer to Appendix A for a detailed outline of the BCSM equations and parameters). In GLM, the clear sky value is reduced according to the amount of clouds, C, according to:

$$f(C) = 0.66182\, C^2 - 1.5236\, C + 0.98475 \tag{8}$$

which is based on a regression of cloud data from Perth Airport, compared against nearby sensor data (R^2 = 0.952; see also Luo *et al.*, 2010).

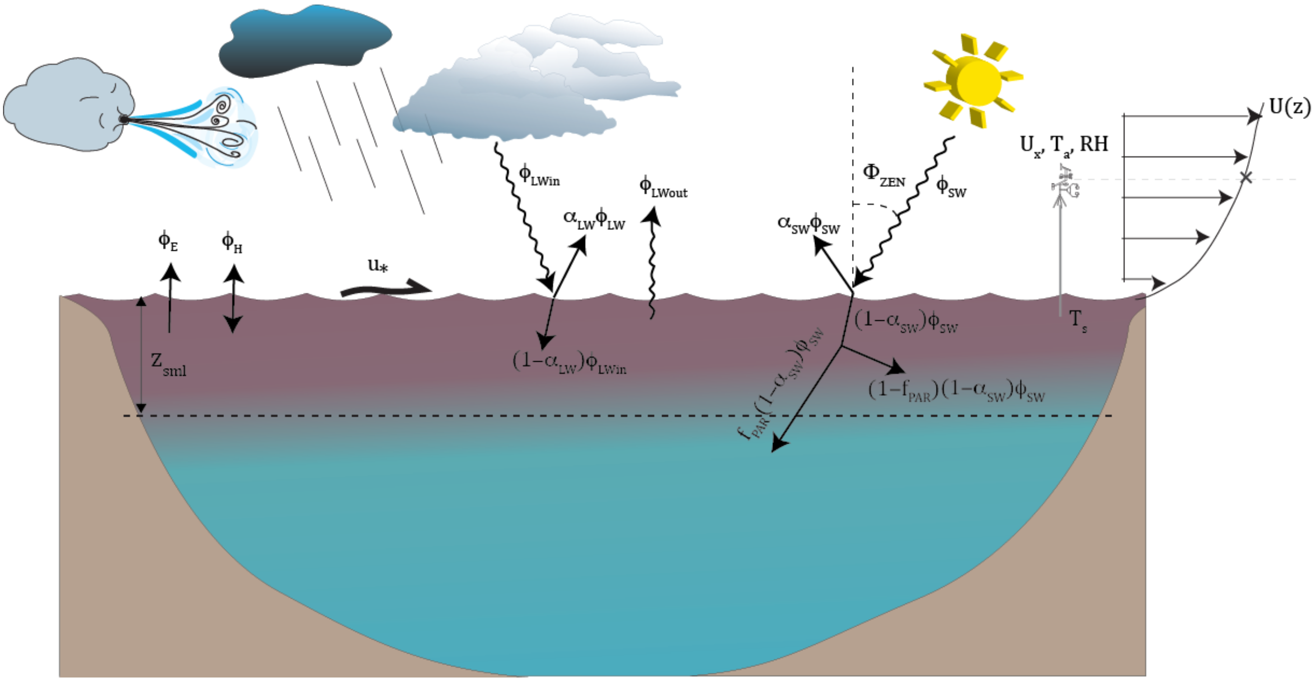

Figure 2: Schematic of a surface heat fluxes impacting the surface mixed layer (sml).

The albedo, α_{SW}, is the reflected fraction of $\hat{\phi}_{SW}$, with several options via `radmode` in `glm.nml`:

Option 1 : Daily approximation, Hamilton & Schladow (1997)

$$\alpha_{SW} = \begin{cases} 0.08 + 0.02\, sin\left[\frac{2\pi}{365}d - \frac{\pi}{2}\right] & : northern\ hemisphere \\ 0.08 & : equator \\ 0.08 - 0.02\, sin\left[\frac{2\pi}{365}d - \frac{\pi}{2}\right] & : southern\ hemisphere \end{cases} \quad (9a)$$

Option 2 : Briegleb *et al.*, (1986)

$$\alpha_{SW} = \frac{1}{100}\left(\frac{2.6}{1.1cos(\Phi_{zen})^{1.7} + 0.065} + 15[cos(\Phi_{zen}) - 0.1][cos(\Phi_{zen}) - 0.5][cos(\Phi_{zen}) - 1]\right) \quad (9b)$$

Option 3 : Yajima & Yamamoto (2014)

$$\alpha_{SW} = 0.001\ \mathrm{RH}\,[\cos(\Phi_{zen})]^{0.33} - 0.001\ U_x\,[\cos(\Phi_{zen})]^{-0.57} - 0.001\ \varsigma\,[\cos(\Phi_{zen})]^{0.829} \quad (9c)$$

where d is the day of the year, and Φ_{zen} is the solar zenith angle (radians) as outlined in Appendix A, RH is the relative humidity and ς is the atmospheric diffuse radiation. The 2nd (oceanic) and 3rd (lacustrine) options allow for diel and seasonal variation of albedo from approximately 0.01 to 0.4 depending on the sun-angle (Figure 3).

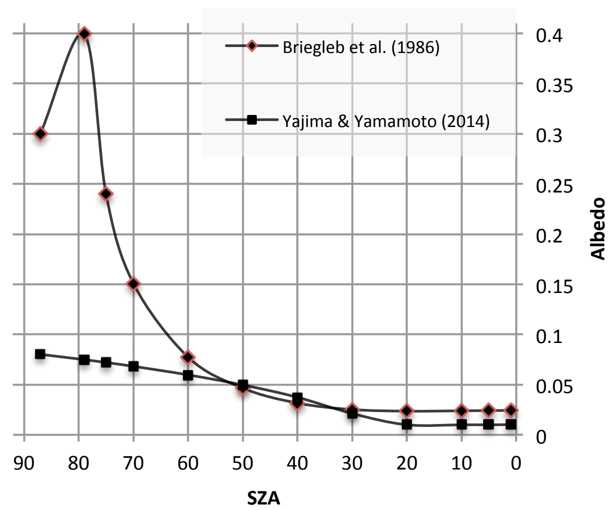

Figure 3: Variation of albedo (α_{SW}) with solar zenith angle (SZA = $2\pi\,\Phi_{zen}/180$, degrees) for `radmode` 2 and 3.

Shortwave radiation penetration into the lake and through the layers is modelled according to the Beer-Lambert Law:

$$\phi_{SW}(z) = (1 - \alpha_{SW})\, f_{SW} f_{PAR}\, \hat{\phi}_{SW}\, exp[-K_w z] \quad (10)$$

where z is the depth of the layer from the surface, f_{SW} is a scaling factor that may be applied and adjusted as part of the calibration process, and K_w is the light extinction coefficient (m^{-1}). K_w may be set by the user as constant or linked to the water quality model (e.g. FABM or AED2) in which case the extinction coefficient will change as a function of depth and time according to the dissolved and particulate constituents. In the model, Beer's Law is only applied for the photosynthetically active fraction (PAR), f_{PAR}, which is 45% of the incident light. The amount of light heating the surface layer, ϕ_{SW_S}, is therefore the above photosynthetically average fraction that enters across z_{SML}, plus the remaining $(1 - f_{PAR})$ fraction which accounts for the fact that near infra-red and ultraviolet bandwidths of the incident shortwave tend to have significantly higher attenuation coefficients (Kirk, 1994).

In some applications the extent to which the benthos has a suitable light climate is a good indicator of benthic productivity, and a proxy for the type of benthic habitat that might emerge. GLM predicts the benthic area of the lake that exceeds a user defined light intensity, $\phi_{BEN_{crit}}$.

$$A_{BEN} = A_s - A(h_{BEN}) \tag{11}$$

where $h_{BEN} = h_{SURF} - z_{BEN}$, and z_{BEN} is calculated from Beer's law:

$$z_{BEN} = ln\left[\frac{\phi_{BEN_{crit}}}{\phi_{SW_S}}\right]\frac{-1}{K_w} \tag{12}$$

The daily average benthic area is reported in the lake.csv summary file as a percentage (A_{BEN}/A_s).

Longwave radiation

Longwave radiation can either be specified as net flux, incoming flux or if there is no radiation data from which longwave radiation can be computed, then it may be calculated by the model internally based on the cloud cover fraction and air temperature. Net long wave radiation is described as:

$$\phi_{LW_{net}} = \phi_{LW_{in}} - \phi_{LW_{out}} \tag{13}$$

where

$$\phi_{LW_{out}} = \varepsilon_w \sigma [T_s + 273.15]^4 \tag{14}$$

and σ is the Stefan-Boltzman constant and ε_w the emissivity of the water surface, assumed to be 0.985. If the net or incoming longwave flux is not provided, the model will compute the incoming flux from:

$$\phi_{LW_{in}} = (1 - \alpha_{LW})\, \varepsilon_a^*\, \sigma\, [T_a + 273.15]^4 \tag{15}$$

where α_{LW} is the long-wave albedo (0.03), and the emissivity of the atmosphere is computed considering emissivity of cloud-free conditions (ε_a), based on air temperature and humidity, extended to account for reflection from clouds, such that $\varepsilon_a^* = f(T_a, C)$ calculated from (Henderson-Sellers, 1986):

$$\varepsilon_a^* = \begin{cases} (1 + 0.275C)\left(1 - 0.261 \exp\left[-0.000777{T_a}^2\right]\right) & \text{Option 1: Idso and Jackson (1969)} \\ (1 + 0.17C^2)\ (9.365\times10^{-6}[T_a + 273.15]^2) & \text{Option 2: Swinbank (1963)} \\ (1 + 0.275C)\ 0.642\left(\frac{e_a}{T_a}\right)^{1/7} & \text{Option 3: Brutseart (1975)} \\ \left[(1 - C^{2.796})\ 1.24\left(\frac{e_a}{T_a}\right)^{\frac{1}{7}} +\ 0.955\ C^{2.796}\right] & \text{Option 4: Yajima and Yamamoto (2014)} \end{cases} \tag{16}$$

where, C is the cloud cover fraction (0-1), and options 1-4 are chosen via the `cloudmode` variable. Note that cloud cover is typically reported in octals (1-8) with each value depicting a fraction of 8. So a value of 1 would correspond to a fraction of 0.125. Some data may also include cloud type and their respective heights. If this is the case, good results have been reported by averaging the octal values for all kinds of cloud cover to get the total cloud cover average value.

If longwave radiation data does not exist and cloud data is also not available, but solar irradiance is measured, then it is possible to use get GLM to compare the measured and theoretical (BCSM) solar irradiance in to approximate the cloud fraction. This option utilises the above relation in Eq 8 to compute $\hat{\phi}_{SW}$ and clouds are approximated by assuming that $\hat{\phi}_{SW_{OBS}}/\hat{\phi}_{SW_{BCSM}} = f(C)$. Please note that if neither shortwave or longwave radiation are provided, then the model will use the BCSM to compute incoming solar irradiance and cloud cover will be assumed to be 0.

Sensible and latent heat transfer

The model accounts for the surface fluxes of sensible heat and latent heat using commonly adopted bulk aerodynamic formulae. For sensible heat:

$$\phi_H = -\rho_a c_p C_H U_x (T_s - T_a) \tag{17}$$

where c_p is the specific heat capacity of air (1005 J/kg/°C), C_H is the bulk aerodynamic coefficient for sensible hear transfer (~1.3x10^{-3}), T_a the air temperature (°C) and T_s the temperature of the surface layer (°C). The air density is in kg m^{-3} and computed from $\rho_a = 0.348\,(1 + r)/(1 + 1.61r)\,p/T_a$, where r is the mixing ratio, p is air pressure in hPa and assuming the gas constant.

For latent heat:

$$\phi_E = -\rho_a C_E\,\lambda\,U_x \frac{\kappa}{p}\,(e_s[T_s] - e_a[T_a]) \tag{18}$$

where C_E is the bulk aerodynamic coefficient for latent heat transfer, e_a the air vapour pressure and e_s the saturation vapour pressure (hPa) at the surface layer temperature (°C) and κ is the ratio of molecular weight of water to molecular weight of air (= 0.622). The vapour pressure can be calculated by the following formulae:

$$e_s[T_s] = exp\left[2.3026\left(7.5\frac{T_s}{T_s+237.3}\right) + 0.7858\right] \quad \text{Option 1 : TVA (1972) - Magnus-Tetens}$$

$$e_s[T_s] = exp\left[6.1094\left(\frac{17.625\,T_s}{T_s+243.04}\right)\right] \quad \text{Option 2 : August-Roche-Magnus} \tag{19}$$

$$e_s[T_s] = 10^{\left(9.28603523\,\frac{2322.37885\,T_S}{T_S+273.15}\right)} \quad \text{Option 3 : Tabata (1973) - Linear}$$

$$e_a[T_a] = \frac{RH}{100} e_s[T_a] \tag{20}$$

Correction for non-neutral atmospheric stability

For long time integrations (i.e. seasonal), the bulk-transfer coefficients for momentum, C_D, sensible heat, C_H, and latent heat, C_E, can be assumed approximately constant because of the negative feedback between surface forcing and the water body's temperature response (e.g. Strub and Powell, 1987). At finer timescales (hours to weeks), the thermal inertia of the water body is too great and so the transfer coefficients must be specified as a function of the degree of atmospheric stratification experienced in the internal boundary layer that develops over the water. Monin and Obukhov (1954) parameterised the stratification seen in the air column using the now well-known stability parameter, z/L, which is used to define corrections to the bulk aerodynamic coefficient C_H and C_E, using the numerical scheme presented in Appendix B. The corrections may be optionally applied in the model, and requires measurement of windspeed, air temperature and relative humidity within the internal boundary layer over the lake surface and specification at an hourly resolution.

Still-air limit

The above formulations only apply so long as sufficient wind exists and creates a defined boundary layer over the surface of the water. As the wind tends to zero (the 'still-air limit') equations (16-17) are no longer appropriate as they do not account for free-convection directly from the water surface. This is a relatively important phenomenon for small dams, ponds and wetlands since they tend have small fetches that limit the build up of wind speed, and they can have surface temperatures warmer than the atmosphere for considerable periods, and they are often sheltered from the wind.

Therefore, in some lakes we need to augment Eqs 16-17 with additional calculations to ensure that low wind-speed results are better captured. The flux estimates can be modified by calculating the evaporative and sensible heat flux values for $U_x = 0$ and the given U_x and taking the maximum magnitude of this pair as the result, *i.e.*,

$$\phi^*_{H,E} = \max\,(\phi_{E,H}, \phi_{E,H_0}) \tag{21}$$

where ϕ_0 is the zero-wind flux, and applies for both evaporative and sensible heat fluxes. $\phi_{E,H}$ is calculated from the equations outlined above and ϕ_0 calculations are given below. The two zero-wind speed heat flux equations are taken from TVA (1972), but modified slightly to return power flux densities in SI units (*i.e.*, Wm^{-2}). The zero wind speed evaporative mass flux calculation is described as:

$$\phi_{E_0} = \rho_s \, \lambda \, \alpha_e (C_0 - C_a) \tag{22}$$

$$\phi_{H_0} = \alpha_h (T_s - T_a)$$

$$\alpha_e = 2.283 \times 10^{-3} \, \xi \, \frac{v}{c_p \rho_s} \left[g \, \frac{|\rho_a - \rho_o|}{\rho_a \nu \, a} \right]^{1/3} \tag{23}$$

$$\alpha_h = 2.283 \times 10^{-3} \, \xi \, v \left[g \, \frac{|\rho_a - \rho_o|}{\rho_a \nu \, a} \right]^{1/3}$$

where $C = \kappa \, e/p$, with the appropriate vapour pressure values, *e*, for both surface and ambient atmospheric values. Here, v is the molecular heat conductivity of air (0.1 kJ m^{-1} hr^{-1} K^{-1}), ν is the kinematic viscosity of the air (0.0548 m^2 hr^{-1}], ρ_o is the density of the saturated air at the water surface temperature, ρ_s is the density of the surface water, ξ is a roughness correction coefficient for the lake surface (0.5), a is the molecular heat diffusivity of air (0.077 m^2 hr^{-1}). Note that the impact of low wind speeds on the drag coefficient is captured by the modified Charnock relation (Eq. A24), which includes an additional term for the smooth flow transition (see also Figure A1).

Wind-sheltering

Hipsey *et al.* (2003) presented a simple adjustment to the bulk transfer equation to account for the effect of wind-sheltering around small dams. The method employs the use of the shelter index which is well suited to one-dimensional application by accounting for the length scale associated with the vertical obstacle relative to the horizontal length scale associated with the dam itself (see also Condie and Webster, 2001). A modified form of the shelter index approximation has been implemented that reduces the effective surface area for heat and momentum fluxes as:

$$A_E = A_S \tanh \left(\frac{A_S}{A_C} \right) \tag{24}$$

where A_C is the critical area. In GLM, the ratio of the effective area to the total area of the lake A_E/A_S is then used to scale U_x as a means of capturing the average wind speed over the entire lake surface.

Snow and ice dynamics

The algorithms for GLM ice and snow dynamics are based on previous ice modelling studies (Patterson and Hamblin, 1988; Gu and Stefan, 1993; Rogers *et al.*, 1995; Vavrus *et al.*, 1996; Launiainen and Cheng, 1998). To solve the heat transfer equation, the ice model uses a quasi-steady assumption that the time scale for heat conduction through the ice is short relative to the time scale of meteorological forcing (Patterson and Hamblin, 1988; Rogers *et al.*, 1995).

The steady-state conduction equations, which allocate shortwave radiation into two components, a visible (A1=70%) and an infra-red (A2=30%) spectral band, which are used with a three-component ice model that includes blue ice (or black ice), snow ice (or white ice) and snow (see Eq. 1 and Fig. 5 of Rogers *et al.*, 1995). Snow ice is generated in response to flooding, when the mass of snow that can be supported by the ice cover is exceeded (see Eq. 13 of Rogers *et al.*, 1995). By assigning appropriate boundary conditions to the interfaces and solving the quasi-steady state of heat transfer numerically, we determine the upward conductive heat flux between the ice or snow cover and the atmosphere, ϕ_0. The estimation of ϕ_0 involves the application of an empirical equation (Ashton, 1986) to estimate snow conductivity (Ks) from its density, where the density of snow is determined as outlined in Figure 4.

At the ice (or snow) surface, a heat flux balance is employed to provide the condition for surface melting,

$$\begin{aligned} \phi_0(T_0) + \phi_{net}(T_0) &= 0 \qquad && T_0 < T_m \\ &= -\rho L \frac{dh_i}{dt} \qquad && T_0 = T_m \end{aligned} \tag{25}$$

where L is the latent heat of fusion (see physical constants, Table 2), h_i is the height of the upper snow or ice layer, t is time, ρ is the density of the snow or ice, determined from the surface medium properties, T_0 is the temperature at the solid surface, T_m is the melt-water temperature (0°C) and $\phi_{net}(T_0)$ is the net incoming heat flux, at the solid surface:

$$\phi_{net}(T_0) = \phi_{LWin} - \phi_{LWout}(T_0) + \phi_H(T_0) + \phi_E(T_0) + \phi_R(T_0) \tag{26}$$

where ϕ_{LWin} and ϕ_{LWout} are incoming and outgoing longwave radiation, ϕ_H and ϕ_E are sensible and evaporative heat fluxes between the solid boundary and the atmosphere, and ϕ_R is the heat flux due to rainfall. These heat fluxes are calculated as above with modification for determination of vapor pressure over ice or snow (Gill, 1982) and the addition of the rainfall heat flux (Rogers *et al.*, 1995). T_0 is determined using a bilinear iteration until surface heat fluxes are balanced (i.e. $\phi_0(T_0) = -\phi_{net}(T_0)$) and T_0 is stable (± 0.001°C). In the presence of ice (or snow) cover, surface temperature $T_0 > T_m$ indicates that energy is available for melting. The amount of energy for melting is calculated by setting $T_0 = T_m$ to determine the reduced thickness of snow or ice (as shown in Eq 25).

Accretion or ablation of ice is determined through the heat flux at the ice-water interface, q_f,. Solving for heat conduction through ice yields:

$$q_f = q_0 - A_1\hat{\phi}_{SW}(1 - \exp[-K_{s1}h_{snow} - K_{w1}h_{white} - K_{b1}h_{blue}]) - A_2\hat{\phi}_{SW}(1 - \exp[-K_{s2}h_{snow} - Kh_{white} - K_{b2}h_{blue}]) - Q_{white}h_{snow} \tag{27}$$

where $\hat{\phi}_{SW}$ is the shortwave radiation penetrating the surface, K refers to the light attenuation coefficient of the ice and snow components designated with subscripts s, w and e for snow, blue ice and snow ice respectively, and h refers to the thickness of snow, white (snow ice) and blue ice. Q_{white} is a volumetric heat flux for formation of snow ice, which is given in Eq. 14 of Rogers *et al.* (1995). Ice and snow light attenuation coefficients in GLM are fixed to the same values as those given by Rogers *et al.* (1995). Reflection of shortwave radiation from the ice or snow surface is a function of surface temperature and ice and snow thickness (see Table 2, Vavrus *et al.*, 1996); values of albedo derived from these functions vary from 0.08 to 0.6 for ice and from 0.08 to 0.7 for snow.

The imbalance between q_f and the heat flux from the water to the ice, q_w, gives the rate of change of ice thickness at the interface with water:

$$\frac{dh_{blue}}{dt} = \frac{q_f - q_w}{\rho_{blue}L} \tag{28}$$

where ρ_{blue} is the density of blue ice and q_w is given by a finite difference approximation of the conductive heat flux from water to ice:

$$q_w = -K_m\frac{\Delta T}{\Delta z}, \tag{29}$$

where K_m is molecular conductivity and ΔT is the temperature difference between the surface water and the bottom of the ice, which occurs across an assigned depth Δz. A value for Δz of 0.5 m is usual, based on the reasoning given in Rogers *et al.* (1995) and the typical vertical resolution of a model simulation (0.125 – 1.5 m). Note that a wide variation in techniques and values is used to determine the basal heat flux immediately beneath the ice pack (e.g., Harvey, 1990).

Figure 4 shows the overall algorithm approach to update ice cover, snow cover and water depth. The ice cover equations are applied when water temperature first drops below 0 °C. The ice thickness is set to its minimum value of 0.05 m, which is suggested by Patterson and Hamblin (1988) and Vavrus *et al.* (1996). The need for a minimum ice thickness relates primarily to horizontal variability of ice cover during the formation and closure periods. The ice cover equations are discontinued and open water conditions are restored in the model when the thermodynamic balance first produces ice thickness < 0.05 m. The effects of snowfall, rainfall, and compaction of snow are described through appropriate choice of one of several options, depending on the air temperature and whether ice or snow is the upper boundary (Figure 4).

Density of fresh snowfall is determined as the ratio of measured snowfall height to water-equivalent height, with any values exceeding the assigned maximum snow density (ρ_{max} = 300 kg m^{-3}) truncated to the upper limit. The snow compaction model is based on the exponential decay formula of McKay (1968), with selection of snow compaction parameters based on air temperature (Rogers *et al.*, 1995) as well as on rainfall or snowfall. The approach of snow compaction used by Rogers *et al.* (1995) is to set the residual snow density to its maximum value when there is fresh snowfall. This method is found to produce increases in snow density that are too rapid when there is only light snowfall. As a result a gradual approach to increasing snow compaction is adopted.

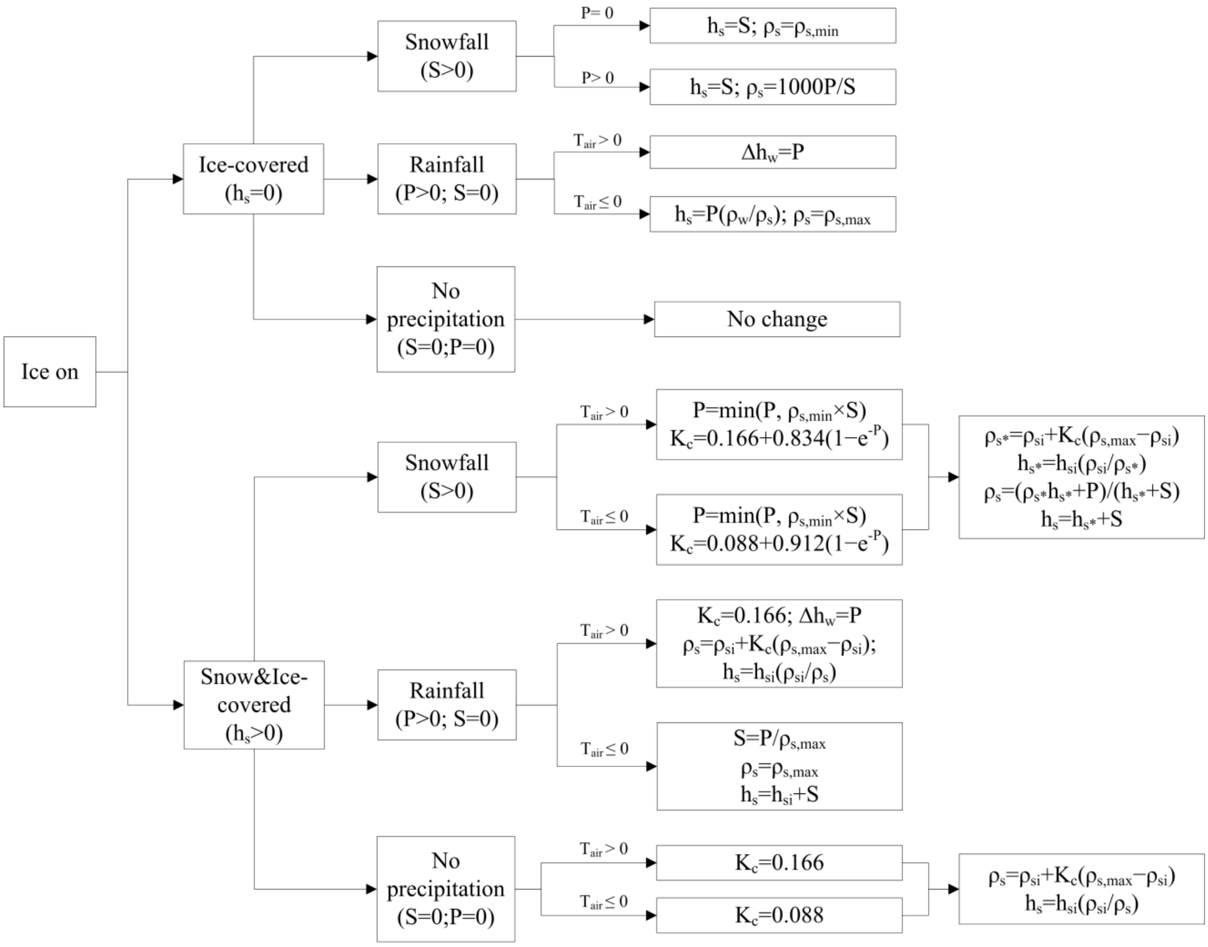

Figure 4: Decision tree to update ice cover, snow cover and water depth according to snow compaction, rainfall (*P*) and snowfall (*S*) on each day, and depth of snow cover (h_{si}) and snow density (ρ_{si}) for the previous day. Refer to Table 1 for definitions of other variables.

Stratification and vertical mixing

Surface Mixed Layer:

GLM works on the premise that the balance between the available energy, E_{TKE}, and the required energy to undergo mixing, E_{PE}, provides for the surface mixed layer (SML) deepening rate dz_{SML}/dt. For an over view of the dynamics readers are referred to early works on bulk mixed layer depth models by Kraus and Turner (1967) and Kim (1976), later more fully extended by Imberger & Patterson (1981) which is the basis for the model design. In this model, the available kinetic energy is calculated due to contributions from wind stirring, shear production between layers, convective overturn, and Kelvin-Helmholtz (K-H) billowing.

They may be combined and summarised for E_{TKE} as (Hamilton and Schladow, 1997):

$$E_{TKE} = \underbrace{0.5 C_K (w_*^3)\,\Delta t}_{convective\ overturn} + \underbrace{0.5 C_K (C_W\, u_*^3)\,\Delta t}_{wind\ stirring} + \underbrace{0.5\, C_S \left[u_b^2 + \frac{u_b^2}{6}\frac{d\xi}{dz_{sml}} + \frac{u_b \xi}{3}\frac{du_b}{dz_{sml}} \right]}_{\substack{shear\ production \\ K-H\ production}} \Delta z_{k-1} \tag{30}$$

where and ξ is the K-H billow length scale (described below), u_b is the shear velocity at the interface of the mixed layer, and C_K, C_W, and C_S are mixing efficiency constants. The energy required to lift up water at the bottom of the mixed layer, denoted here as the layer $k-1$, with thickness Δh_{k-1}, and accelerate it to the mixed layer velocity is required for mixing to occur. This also accounts for energy consumption associated with K-H production and expressed as, E_{PE}:

$$E_{PE} = \left[\underbrace{0.5 C_T (w_*^3 + C_W\, u_*^3)^{2/3}}_{acceleration} + \underbrace{\frac{\Delta\rho}{\rho_o} g\, z_{SML}}_{lifting} + \underbrace{\frac{g\xi^2}{24\rho_o}\frac{d(\Delta\rho)}{dz_{sml}} + \frac{g\xi\Delta\rho}{12\rho_o}\frac{d\xi}{dz_{sml}}}_{K-H\ consumption} \right] \Delta z_{k-1} \tag{31}$$

where, z_{SML} is the thickness of the surface mixed layer. To numerically resolve the above equations we must sequentially compute the different components of the above expressions in light of the layer structure, and GLM follows the algorithm in Imberger and Patterson (1981) whereby we first undertake cooling and combination of layers due to convection, then undertake stirring and then computing shear and K-H mixing.

To compute mixing due to convective cooling we compute the value for w_*, which is the turbulent velocity scale associated with convection. The model adopts the algorithm used in Imberger and Patterson (1981; Eq 32), whereby the potential energy that is released by mixed layer deepening is computed by looking at the moments of the different layers in the surface mixed layer (from layer K to N_{LEV}):

$$w_*^3 = \frac{g}{\rho_{SML}\,\Delta t}\left(\sum_{k=K}^{N_{LEV}} [\rho_k\, \Delta z_k\, \widetilde{h_k}] - \widetilde{h_{SML}} \sum_{k=K}^{N_{LEV}} [\rho_k\, \Delta z_k\,] \right) \tag{32}$$

where ρ_{SML} is the mean density of the mixed layer including the combined layer, ρ_k is the density of the k^{th} layer, Δz_k is the height difference between two consecutive layers within the loop ($\Delta z_k = h_k - h_{k-1}$), $\widetilde{h_k}$ is the mean height of layers to be mixed ($\widetilde{h_k} = 0.5[\,h_k + h_{k-1}]$), and $\widetilde{h_{SML}}$ is the epilimnion (surface mixed layer) mid height, calculated from: $\widetilde{h_{SML}} = 0.5[\,h_{SURF} + h_{K-1}]$.

The velocity scale u_* is associated with wind stress and calculated according to the wind strength:

$$u_*{}^2 = C_D U_x^2 \tag{33}$$

where C_D is the drag coefficient for momentum. The model first computes the following check to see if the stirring energy is enough to overcome the energy required to mix the k-1 layer, i.e., mixing occurs if:

$$C_K (w_*^3 + C_W\, u_*^3)\,\Delta t \;\geq\; (g'_k\, z_{SML} + \; C_T (w_*^3 + C_W\, u_*^3)^{2/3})\Delta z_{k-1} \tag{34}$$

and $g'_k = \frac{\Delta\rho}{\rho_o}$ is the reduced gravity between the mixed layer and k-1 layer. If the condition is not met the energy is stored for the next time-step.

Once stirring is completed mixing due to velocity shear is applied. Velocity shear at the interface is approximated from:

$$u_b = \frac{u_*{}^2 t}{z_{sml}} + u_o \tag{35}$$

where t is a time value over which it has been operating, considered relative to t_{shear} which is the time beyond which shear production doesn't occur (ie., $u_b = 0$ if the time exceeds t_{shear}). This cut off time assumes use of only the energy produced by shear at the interface during the half seiche period, T_i, and modified to account for damping:

$$t_{shear} = T_i \left(1 + 0.59 \left[1 - cosh\left(\frac{T_d}{T_i} - 1 \right)^{-1} \right] \right) \tag{36}$$

where T_d is the time-scale of damping (see Spigel, 1978). The wave period is approximated based on the stratification as $T_i = L_{META}/2c$, where L_{META} is the length of the domain at the thermocline and c is the internal wave speed. Once the velocity is computed, the energy for mixing from velocity shear is compared to that required for lifting and accelerating the next layer down and layers are combined:

$$0.5\, C_S \left[\frac{u_b^2 (\widetilde{z_{SML}} + \Delta\xi)}{6} + \frac{u_b \xi \Delta u_b}{3} \right] + \left[g'_k \xi \left(\frac{\xi \Delta z_{k-1}}{24 z_{SML}} - \frac{\Delta\xi}{12} \right) \right] \;\geq\; (g'_k\, z_{SML} + \; C_T (w_*^3 + C_W\, u_*^3)^{2/3})\Delta z_{k-1} \tag{37}$$

where the K-H length scale is $\xi = C_{KH} u_b^2 / g'_{EH}$, and $\Delta\xi = 2\, C_{KH}\, u_b\, \Delta u_b / g'_{EH}$; in this case the reduced gravity is computed from the difference between the epilimnion and hypolimnion, and C_{KH} is a measure of the billow mixing efficiency.

Once shear mixing is done, the model checks the resultant density interface to see if it is unstable to shear (ie. K-H billows would be expected to form). This occurs if the gradient is less that the K-H length scale, and then if K-H mixing is required layers are further split and subject to mixing using an algorithm similar to above.

Deep Mixing:

Mixing below the SML in lakes, in the deeper stratified regions of the water column, is modelled using a characteristic vertical diffusivity, $K_Z = K_\varepsilon + K_m$, where K_m is the fixed molecular diffusivity of scalars. The model adopted in GLM is based on the derivation by Weinstock (1981) that is described as being suitable for regions displaying weak or strong stratification, whereby diffusivity increases with dissipation and decreases with heightened stratification:

$$K_z = \frac{\alpha_{TKE}\varepsilon_{TKE}}{N^2 + 0.6\, {k_{TKE}}^2 {u_*}^2} \tag{38}$$

where α_{TKE} is the mixing efficiency of hypolimnetic TKE (~0.8 in Weinstock, 1981) and k_{TKE} is the turbulence wavenumber:

$$k_{TKE} = \frac{12.4\, A_{top}}{\tilde{V}\, \Delta z_{top}\, 10^3} \tag{39}$$

and $u_* = \sqrt{1.612 \times 10^{-6}\, {U_x}^2}$. The term N^2 is the Brunt–Väisälä (buoyancy) frequency defined as:

$$N^2 = \frac{g\Delta\rho}{\rho\Delta z} \approx \left[\frac{g(\rho_{i+2} - \rho_{i-2})}{\rho_{ref}(h_{i+2} - h_{i-2})}\right] \tag{40}$$

Estimating the turbulent dissipation rate can be complex but GLM adopts the simple approach as described in Fischer et al. (1980) where a "net dissipation" is approximated by assuming dissipation is in equilibrium with energy inputs from external drivers:

$$\varepsilon_{TKE} \approx \overline{\varepsilon_{TKE}} = E_{WIND} + E_{INFLOW} \tag{41}$$

which is expanded and calculated per unit volume as:

$$\varepsilon_{TKE} = \underbrace{\frac{1}{(\tilde{V}\bar{\rho})10^3}\frac{m\, C_D \rho_a\, f_S\, {U_x}^3\, A_l}{10^6}}_{rate\ of\ working\ by\ wind} + \underbrace{\frac{1}{(V_{mix}\bar{\rho})10^3}\sum_i^{N_{INF}} g\, \Delta\rho_i\, Q_i (h_{top} - h_i)}_{rate\ of\ working\ done\ by\ inflows} \tag{42}$$

The diffusivity is calculated according to Eq 42, but since the dissipation is assumed to concentrate close to the level of strongest stratification, the "mean" diffusivity is modified to decay exponentially with distance from the thermocline:

$$K_{z_l} = \begin{cases} 0 & h_l \geq (h_{top} - z_{mix}) \\ K_z\ exp\left[\dfrac{-(h_{top} - z_{mix} - h_l)^2}{\sigma}\right] & h_i < (h_{top} - z_{mix}) \end{cases} \tag{43}$$

where is the σ variance the N^2 distribution below h_{mix} and scales the depth over which mixing decays.

Once the diffusivity is approximated, the diffusion of any scalar, C, between two layers is numerically accounted for by the following mass transfer expressions:

$$C_{i+1} = \bar{C} + \frac{\exp(-f)\Delta z_i \Delta C}{(\Delta z_{i+1} + \Delta z_i)} \tag{44}$$

$$C_i = \bar{C} - \frac{\exp(-f)\Delta z_{i+1} \Delta C}{(\Delta z_{i+1} + \Delta z_i)}$$

where $\bar{C}$ is the weighted mean concentration of C for the two layers, and ΔC is the concentration difference between them. f is related to the diffusivity according to:

$$f = \frac{K_{z_{i+1}} + K_{z_i}}{(\Delta z_{i+1} + \Delta z_i)^2}\Delta t \tag{45}$$

The above diffusion algorithm is run once up the water column and once down the water column as a simple explicit method for capturing diffusion to both the upper and lower layers.

Inflows and outflows

Inflows can be specified as surface runoff from the surrounding lake domain (described above, Eq 5), rivers entering at the surface of the lake or submerged inflows. Any number of inflows to the lake body can be specified and these are applied at the end of the sub-daily loop, i.e. once a day.

Three forms of outflows are included in GLM, ground water seepage, outflow from a specified depth or overflow.

River inflows

For river inflows, depending on the density of the river water, the inflow will form a positive or negatively buoyant intrusion. As the inflow crosses layers it will entrain water out of them, until it reaches a level of neutral buoyancy and undergoes insertion. Therefore, when it reaches its point of neutral buoyancy a new layer of thickness dependent on the inflow volume at that time (including additions from entrainment) is created. Following insertion, the inflow layer may then amalgamate with adjacent layers depending on numerical criteria within the model for combining or splitting layers.

The rate of entrainment of the intrusion, E, can be calculated in a number of ways. For simplicity in GLM, the rate has been adapted from the first approximation in Fisher et al. (1979):

$$E = 1.6 \frac{{C_{D_i}}^{3/2}}{Ri} \tag{46}$$

where C_{D_i} is the user specified drag coefficient for the inflow. The Richardson's number is adapted from Fisher et al. (1979) as:

$$Ri = \frac{C_{D_i}\left(1 + 0.21\sqrt{C_{D_i}}\,\sin\alpha_{inf}\right)}{\sin\alpha_{inf}\tan\phi_{inf}} \tag{47}$$

where α_{inf} is the stream half angle and ϕ_{inf} is the slope of the inflow at the point where it meets the water body (Figure 5).

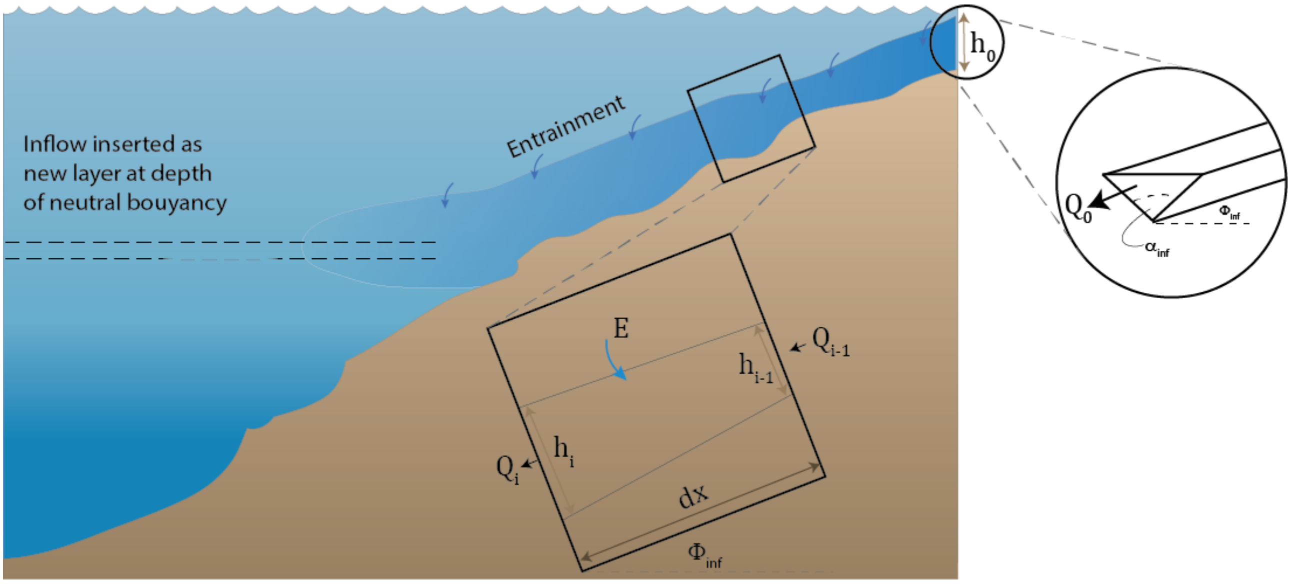

Figure 5: Schematic showing inflow insertion, entrainment and slope, ϕ_{inf} and half angle, α_{inf} of inflowing rivers.

As the inflow parcel travels through the layers, the increase in inflow thickness due to entrainment is estimated as:

$$h_i = 1.2 E dx + h_{i-1} \tag{48}$$

where h_i is the inflow thickness, E is the entrainment rate and dx is the distance travelled by the inflowing water, calculated from the flow rate and inflow thickness. The initial estimation of the intrusion height is computed from (Imberger and Patterson, 1981; Antenucci *et al.*, 2005):

$$h_0 = \left(2Q_{inf}{}^2 \frac{Ri}{g'_{inf}{}'} \tan^2\phi_{inf}\right)^{1/5} \tag{49}$$

where Q_{inf} is the inflow rate provided as a boundary condition and g' is the reduced gravity of the inflow given as:

$$g'_{inf} = g\frac{(\rho_{inf} - \rho_s)}{\rho_s} \tag{50}$$

where ρ_{inf} is the density of the inflow and ρ_s the density of the surface layer. The distance travelled by the inflow aliquot, dx, is estimated as the distance travelled in the vertical and the slope of the inflow river, ϕ_{inf} and given by:

$$dx = \frac{dz}{\sin\phi_{inf}} \tag{51}$$

where dz is the distance travelled in the vertical. The velocity of the inflow aliquot for that day is then calculated as:

$$u = h_i^2\frac{Q_{inf}}{\tan\alpha} \tag{52}$$

Following conservation of mass, the flow is estimated to increase according to (Imberger and Patterson, 1981; Antenucci *et al.*, 2005):

$$Q_i = Q_{i-1}\left[\left(\frac{h_i}{h_{i-1}}\right)^{5/3} - 1\right] \tag{53}$$

The above entrainment and insertion algorithm is repeated fro each inflow. Aside from importing mass into the lake, river inflows also contribute turbulent kinetic energy to the hypolimnion as discussed in the Deep Mixing section above (e.g., Eq 42).

Submerged inflows

Submerged inflows are inserted at the specified depth with zero entrainment. The submerged inflow layer is then mixed with adjacent layers above or below depending on the density difference until neutral buoyancy is reached.

Withdrawals

Outflows can be specified at any depth over the water column and will draw water from the adjacent layer, layers above or below depending on the strength of discharge and stability of the water column according to the following algorithms. The three types of outflow, seepage, withdraw and overflow all use the same algorithms with overflow volume calculated by the volume of water in excess of maximum storage once rainfall, evaporation and all inflows and outflows have been accounted for.

The thickness of the withdrawal layer is dependent on the calculation of the internal Froude (Fr) and Grashof (Gr) numbers and a parameter, *R* (Fisher et. L 1979):

$$Fr = \frac{Q_{outf}}{N_{outf}^2 W_{outf} L_{outf}^2} \tag{54}$$

$$Gr = \frac{N_{outf}^2 A_i^2}{v_{outf}^2} \tag{55}$$

$$R = Fr\,Gr^{1/3} \tag{56}$$

Where W_{outf}, L_{outf} and A_i are the width, length and area of the lake at the outlet elevation, and v_{outf}^2 is the vertical diffusivity of momentum averaged over the withdrawal layer and the Brunt- Väisälä frequency averaged over the thickness of the withdrawal layer, N_{outf}^2 is calculated as:

$$N_{outf}^2 = \frac{g}{dz}\frac{\rho_{outf} - \rho_i}{\rho_{outf}} \tag{57}$$

where dz is the thickness of the withdrawal layer, ρ_{outf} is the density of the lake at the height of withdrawal and ρ_i is the density of the lake at the edge of the withdrawal layer.

The thickness of the withdrawal layer is then calculated as follows (Fisher et al. 1978):

$$\delta_{outf} = 2L_{outf}Gr^{-1/6} \tag{58}$$

$$\delta_{outf} = 2L_{outf}Fr^{1/2}$$

The proportion of fluid withdrawn from each layer either above or below the layer of the outlet elevation is determined using a curve that fits the region of fluid drawn in a given time.

To calculate the width and length of the lake at the height of outflow the following assumptions are made:

1. That the lake shape approximates as an ellipse.
2. The ratio of length to width at height of outflow is the same as that at the lake crest.

The length of the lake at the outflow height, L_{outf} and the lake width, W_{outf} are given by:

$$L_{outf} = \sqrt{A_{outf}\frac{4}{\pi}\frac{L_{crest}}{W_{crest}}} \tag{59}$$

$$W_{outf} = L_{outf}\frac{W_{crest}}{L_{crest}}$$

where A_{outf} is the area of the lake at the outflow height, L_{crest} is the length and W_{crest} the width of the lake at the crest height.

Seepage

Seepage of water from the bottom layer is also configurable within the model, for example, as might be required in a wetland simulation. Seepage is configured to leave the lake at a constant rate:

$$\frac{dh_B}{dt} = -G \tag{60}$$

where h_B is the depth of the bottom-most layer at any time, and G is the seepage rate (m day^{-1}). G is constrained within the model to ensure no more than 50% of the layer can be reduced in any one time-step. Note that in shallow simulations, a single layer may form, in which case the surface and bottom later are the same and Eq 4 and 60 are combined.

Bottom stress

Wind-induced resuspension of sediment from the bed of shallow lakes is sporadic and occurs as the waves created at the water surface create oscillatory currents that propagate down to the lake-bed. GLM does not predict resuspension and sediment concentration directly, but computes the bottom shear stress for later use by sediment and water quality modules that are within FABM-AED. Nonetheless, even without this sophistication the model can identify the areal extent and potential for bed-sediment resuspension by computing the area of the lake over which the bed shear stress exceeds some critical value required for resuspension to occur.

To compute the stress at the lake bottom we estimate the surface wave conditions using a simple, fetch-based, steady state wave model (Laenen and LeTourneau, 1996; Ji 2008). The wave geometry (wave period, significant wave height and wave length), is predicted based on the windspeed and fetch over which the waves develop (Figure 6), calculated as:

$$F = 2\sqrt{A_s/_\pi} \tag{61}$$

Using this model, the wave period, T, is calculated from fetch as:

$$T = 7.54\left(\frac{U_x}{g}\right)tanh(\xi)\,tanh\left(\frac{0.0379\left[\frac{gF}{U_x^2}\right]^{0.333}}{tanh(\xi)}\right) \tag{62}$$

where:

$$\xi = 0.833 \left[\frac{g d_{avg}}{U_x^2}\right]^{0.375} \tag{63}$$

and h_{avg} is the average lake depth. Wave length is then estimated from:

$$L = \left[\frac{gT^2}{2\pi}\right] tanh\left(\frac{2\pi\, d_{avg}}{\left[\frac{gT^2}{2\pi}\right]}\right) \tag{64}$$

and wave height from:

$$H_s = 0.283 \left(\frac{U_x^2}{g}\right) tanh(\zeta) tanh\left(\frac{0.00565 \left[\frac{gF}{U_x^2}\right]^{0.5}}{tanh(\zeta)}\right) \tag{65}$$

where

$$\zeta = 0.53 \left[\frac{g d_{avg}}{U_x^2}\right]^{0.75} \tag{66}$$

Based on these properties the orbital wave velocity at depth (in the i th layer) is calculated as:

$$U_{orb_i} = \frac{\pi H_s}{T sinh\left[\frac{2\pi\, d_i}{L}\right]} \tag{67}$$

The total shear stress at the lake bed is calculated as:

$$\tau_i = \frac{1}{2}\, \rho_w \left[\, f_w\, U_{orb_i}{}^2 + \, f_c\, U_{m_i}{}^2 \right] \tag{68}$$

where U_m is the mean velocity of the layer, computed during the mixing calculations (Eq 33). The friction factors use D (a typical particle diameter). For the current stress we compute ($f_w = 0.24/\log(12 d_{avg}/2.5D)$ and for waves, based on:

$$f_w = \exp\left[-5.977 + 5.213 \left(\frac{a}{2.5D}\right)^{-0.19}\right] \quad \text{Option 1 : Laenen and LeTourneau, 1996} \tag{69}$$

$$f_w = 0.00251 \exp\left[5.213 \left(\frac{U_{orb}\, T}{4\pi D}\right)^{-0.19}\right] \quad \text{Option 3 : Kleinhans \& Grasmeijer (2006)}$$

$$f_w = \frac{2\beta g \rho_D D}{U^2 \rho_w} \quad \text{Option 3 : Le Roux (2007)}$$

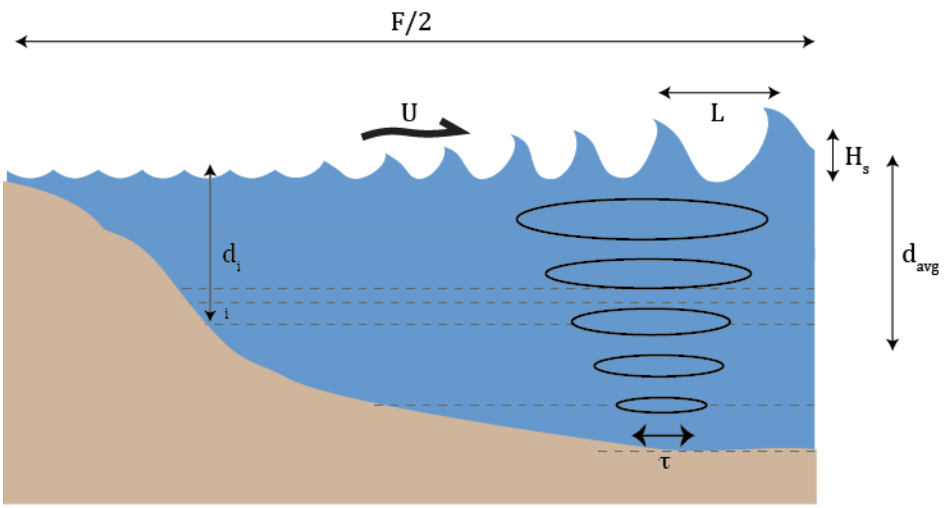

Figure 6: Slope, ϕ_{inf} and half angle, α_{inf} of inflowing rivers.

Table 1. Summary of GLM physical parameters with recommended values and references.

Symbol	glm.nml ID	Description	Units	Default	Reference	Comments
Model Structure						
h_{min}	min_layer_thick	Minimum layer thickness	m	0.5	-	Standardised for multi-lake comparison
h_{max}	max_layer_thick	Maximum layer thickness	m	1.5	-	Should be estimated relative to lake depth.
Lake Properties						
K_w	Kw	Extinction coefficient for PAR radiation	m^{-1}	0.2	Lake specific	Should be measured, e.g. mean of simulation period. Can be estimated from Secchi depth.
A_C	critical_area	Critical area below which wind sheltering may occur	m^2	10^7	Xenopoulos and Schindler (2001)	
Surface Thermodynamics						
C_H	ch	Bulk aerodynamic coefficient for sensible heat transfer	-	0.0013	Fischer et al. (1979)	From Hicks' (1972) collation of ocean and lake data; many studies since use similar values. Internally calculated if atmos stability correction is on.
C_E	ce	Bulk aerodynamic coefficient for latent heat transfer	-	0.0013	Fischer et al. (1979)	
C_M	cd	Bulk aerodynamic coefficient for transfer of momentum	-	0.0013	Fischer et al. (1979)	
λ	-	Latent heat of evaporation	$J\ kg^{-1}$	2.453×10^6	Standard	Not adjustable in glm.nml
ε_a	-	Emissivity of the water surface	-	0.985	Standard	Water only, no ice Ice or snow
σ	-	Stefan-Boltzmann constant	$W\ m^{-2}\ K^{-4}$	5.67×10^{-8}		Not adjustable in glm.nml
Mixing Parameters						
C_K	coef_mix_conv	Mixing efficiency - convective overturn	-	0.2	Yeates & Imberger (2003)	Selected by Yeates et al (2004) from a range given in Spigel et al. (1986)
C_W	coef_wind_stir	Mixing efficiency - wind stirring	-	0.23	Spigel et al. (1986)	From Wu 1973
C_S	coef_mix_shear	Mixing efficiency - shear production	-	0.3	Sherman et al. (1978)	Best fit of experiments reviewed
C_T	coef_mix_turb	Mixing efficiency - unsteady turbulence (acceleration)	-	0.51		
C_{KH}	coef_mix_KH	Mixing efficiency - Kelvin-Helmholtz turbulent billows	-	0.3	Sherman et al. (1978)	"a good rule of thumb..."
C_{HYP}	coef_mix_hyp	Mixing efficiency of hypolimnetic turbulence	-	0.5	Weinstock 1981	General diffusivities in Jellison and Melack (1993)
Inflows & Outflows						
C_D	strmbd_drag	streambed_drag	-	0.016		Set based on inflow stream type
G	seepage_rate	Seepage rate	$m\ day^{-1}$	0		Site specific
Snow & Ice						
K_{w1}	-	Waveband 1, snow ice light extinction	m^{-1}	48.0		
K_{w2}	-	Waveband 2, snow ice light extinction	m^{-1}	20.0		
K_{b1}	-	Waveband 1, blue ice light extinction	m^{-1}	1.5		
K_{b2}	-	Waveband 2, blue ice light extinction	m^{-1}	20.0		
K_{s1}	-	Waveband 1, snow light extinction	m^{-1}	6		
K_{s2}	-	Waveband 2, snow light extinction	m^{-1}	20		
D_z	-	Distance of hear transfer, ice water	m	0.039		

Symbol	glm.nml ID	Description	Units	Default	Reference	Comments
ρ_{white}	-	Density, snow ice	kg m^{-3}	890		
ρ_{blue}	-	Density, blue ice	kg m^{-3}	917		
ρ_{snow}	-	Density, snow	kg m^{-3}	Variable		
c_{pi}	-	Heat capacity, ice	kJ kg^{-1} $°C^{-1}$	2.1		
c_{pw}	-	Heat capacity, ice	kJ kg^{-1} $°C^{-1}$	4.2		
K_c	-	Compaction coefficient	-	Variable		
K_m	-	Thermal conductivity, snow ice	W m^{-1} $°C^{-1}$	2.0		
K_m	-	Thermal conductivity, blue ice	W m^{-1} $°C^{-1}$	2.3		
K_m	-	Thermal conductivity, snow	W m^{-1} $°C^{-1}$	Variable		
K_m	-	Thermal conductivity, sediment	W m^{-1} $°C^{-1}$	1.2		
K_m	-	Thermal conductivity, water	W m^{-1} $°C^{-1}$	0.57		
L	-	Latent heat of fusion	kJ kg^{-1}	0334		
Bottom Stress						
D	-	Typical particle diameter	m			

Setup & Operation

Overview

This section gives a description of the structure of a GLM setup is described. GLM requires a configuration files and several time-series input files and integrates with FABM-AED or AED2 for water quality simulations (Figure 7).

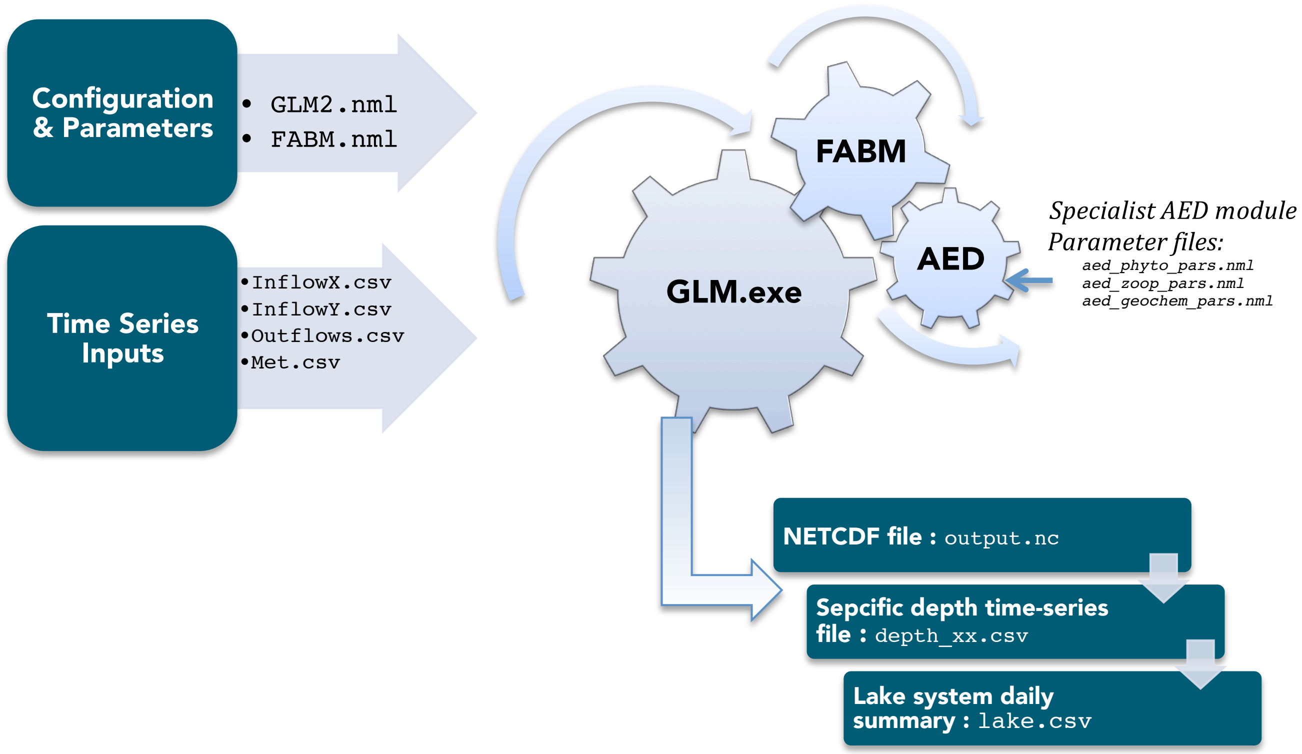

Figure 7: Flow diagram showing the files required for operation of the model.

Input files

Physical model configuration: `glm.nml`

The file `glm.nml` is the main configuration file for the physical model, and some details related to the FABM coupling. The nml file includes detailed description of the different namelist options for each block; if these value are not present default values will be assumed. It is a namelist file with blocks for:

- `&glm_setup`: General simulation info and mixing parameters
- `&wq_setup`: Details about the coupling with the water quality model (eg. FABM or AED2)
- `&time`: Time controls
- `&morphometry`: Lake morphometric information
- `&output`: Specification of output file details (depths, output frequency and variables to write)
- `&init_profiles`: Setting initial conditions (depth profiles) of GLM and WQ variables
- `&meteorology`: Information about surface forcing and meteorology data
- `&inflows`: Information about inflows
- `&outflows`: Information about outflows
- `&bird`: Optional block to input parameters for the Bird solar radiation model

Refer to the example `glm.nml` files for detailed over view of the layout and required information. The key elements are described below.

Meteorological configuration and **met.csv**

A range of options exist for customising the meteorological forcing of the lake simulation.

Key configuration variables users may provide are:

- `met_sw`: Switch to enable (`.true.`) or disable (`.false.`) meteorological forcing.
- `snow_sw`: Switch to enable (`.true.`) or disable (`.false.`) the snow/ice model.
- `rain_sw`: Switch to enable (`.true.`) or disable (`.false.`) rainfall nutrient composition.
- `rad_mode`: Switch to configure the shortwave/longwave radiation sub-model (Table 2).
- `cloud_mode`: Switch to configure the atmospheric longwave emissivity sub-model (Eq 16).
- `albedo_mode`: Switch to configure the shortwave albedo algorithm (Eq 9).
- `atm_stab`: Switch to enable (`.true.`) or disable (`.false.`) non-neutral atmospheric stability.

Details of the meteorological boundary condition data are summarised according to:

- `subdaily`: Determines whether the model expects to read in sub-daily meteorological data.
- `meteo_file`: Name of the csv file containing meteorological data.
- `time_fmt`: Format of the time/data column in the meteorological input file.
- `wind_factor`: Scaling factor that is used to multiply the wind speed data that is read in.
- `rain_factor`: Scaling factor that is used to multiply the rainfall data that is read in.
- `at_factor`: Scaling factor that is used to multiply the air temperature data that is read in.
- `rh_factor`: Scaling factor that is used to multiply the relative humidity data that is read in.
- `sw_factor`: Scaling factor that is used to multiply the shortwave data that is read in.
- `lw_factor`: Scaling factor that is used to multiply the longwave data that is read in.

Details of the parameters used in the model include:

- `ce`: Bulk-transfer coefficient for latent heat flux calculation under neutral conditions.
- `ch`: Bulk-transfer coefficient for sensible heat flux calculation under neutral conditions.
- `cd`: Bulk-transfer coefficient for momentum flux calculation under neutral conditions.

Table 2: Summary of the ways GLM can treat solar radiation and cloud data, as configured through `rad_mode`.

rad_mode	Data required in **met.csv**		Solar data creation and treatment of longwave or cloud data
0	Solar (daily)	Clouds (daily)	Daily solar radiation data is subject to a sine wave disaggregation to get a sub-daily light time-series. The daily total energy input equals the daily value provided by the user. Cloud cover data is used for prediction of longwave radiation.
1	Solar (sub-daily)	Clouds (sub-daily)	Sub-daily solar radiation data is used directly. Cloud cover data is used for prediction of longwave radiation.
2	Solar (sub-daily)	No Cloud data, LongWave provided	Sub-daily solar radiation data is used directly. Clouds are not used in the model, longwave data is expected in `met.csv` and is used directly in the heat balance.
3	Solar (sub-daily)	No Cloud data, No Longwave provided	Sub-daily solar radiation data is used directly. No longwave or cloud data is provide to the model, so GLM will attempt to estimate cloud fraction: $\hat{\phi}_{BC}/\hat{\phi}_{SW} = f(C)$
4	None	Clouds (sub-daily)	Sub-daily solar radiation data is computed using the BCSM model, adjusted for cloud cover: $\hat{\phi}_{BC} = \hat{\phi}_{SW}\, f(C)$ Cloud cover data is used for prediction of longwave radiation
5	None	None	Sub-daily solar radiation data is computed using the BCSM model, and clear-sky values will be assumed. Longwave radiation is predicted with a cloudiness of 0 assumed.

Users must be sure to provide the correct combination of "ShortWave" and "LongWave" or "Clouds" according to their chosen `rad_mode` (Table 4).

The meteorological conditions are provided as a time-series of data with a fixed number of columns, as outlined in Table 3. This maybe included as daily data (`subdaily =.false.`) or at the time-step of the model simulation (eg., hourly) if `subdaily =.true.` It contains seven compulsory columns, and several optional columns after these depending on the user-defined configuration switches for `snow_sw` and `rain_sw` in the `glm.nml` file.

Table 3: Flow diagram showing the files required for operation of the model.

`met.csv` column	Units	Description
(1) TIME `time`	YYYY-MM-DD	Date, specified in the format of `time_fmt` , defaults as: YYYY-MM-DD HH:MM:SS
(2) SHORTWAVE RADIATION `ShortWave`	W/m^2 Required if `rad_mode` = 0, 1, 2 or 3	Daily average shortwave radiation. Note that the daily value is internally distributed to a sub-daily time step by assuming and idealized diurnal cycle.
(3) LONGWAVE RADIATION `LongWave`	W/m^2 Required if `rad_mode` = 2	Longwave radiation input is assumed to be direct incident intensity,.
(3) CLOUD COVER `Clouds`	- Required if `rad_mode` = 0, 1 or 4	Incoming longwave flux, is estimated from cloud cover fraction data
(4) AIR TEMPERATURE `AirTemp`	°C	Daily average air temperature 10m above the water surface
(5) RELATIVE HUMIDITY `RelHum`	%	Daily average relative humidity (0-100%) 10m above the water surface.
(6) WIND SPEED `WindSpeed`	m/s	Daily average wind speed 10m above the water surface
(7) RAINFALL `Rain`	m/day	Daily rainfall depth
(8) SNOWFALL (optional) `Snow`	m/day	Daily snowfall depth (optional – include if `snow_sw` is T)
(9-14) RAINFALL WQ DEPOSITION CONCENTRATIONS (optional)	mg/L	Assumed concentration of WQ variables in the rainfall (optional – include if `rain_sw` is T)

Configuration of inflows and setup of `inflows.csv`

A range of options exist for customising the inflow forcing of the lake simulation, in the `&inflow` section. Any number of inflows can be simulated by the model with the configuration and filenames set in the `glm.nml` file.

Several configuration variables and parameters must be provided:

- `num_inflows`: Number of streams to be simulated. Set to 0 if no streams are included.
- `names_of_strms`: Names of the inflowing streams/rivers, separated by commas.
- `strm_hf_angle`: Steambed half-angle for each inflowing stream (Figure 5), separated by commas.
- `strmbd_slope`: Steambed slope for each inflowing stream (Figure 5), separated by commas.
- `strmbd_drag`: Steambed drag for each inflowing stream (Table 1), separated by commas.
- `submerged`: Flag for each inflow indicating if it is a submerged input, separated by commas.

Details of the inflow boundary condition data are summarised according to:

- `inflow_fl`: Name of the csv file containing the inflow data.
- `time_fmt`: Format of the time/data column in the inflow input file.
- `inflow_factor`: Scaling factor that is used to multiply the inflow data that is read in.
- `inflow_varnum`: Number of variables to be read in for each inflow.
- `inflow_vars`: List and order of variables being read in. Order must be as in the input file.

For each inflow there is an associated inflow file of the format outlined in Table 4. At this stage the file only accepts daily data as the inflow calculation is done once a day. It contains four mandatory columns for time, flow, temperature and salinity, and optional columns for water quality constituents.

Table 4: Flow diagram showing the files required for operation of the model.

`inflow.csv` column	Units	Description
(1) TIME `time`	YYYY-MM-DD	Date, specified in the format of `time_fmt` , defaults as: YYYY-MM-DD HH:MM:SS
(2) INFLOW `flow`	ML/day	Daily flow rate. Convert from m^3/s by multiplying by 86.4.
(3) STREAMFLOW TEMPERATURE `temp`	°C	Average daily streamflow temperature
(4) STREAMFLOW SALINITY `salt`	mg/L	Average daily streamflow salinity
(5 … n_{WQ}+4) STREAMFLOW WATER QUALITY PARAMETER CONCENTRATIONS `aed_oxygen_oxy`	$mmol/m^3$	Average daily streamflow water quality constituent concentrations.

Configuration of outflows and setup of **`outflows.csv`**

Any number of outflow fluxes can be configured and these are set as consecutive columns in the file `outflows.csv` (Table 5). Only daily flow rates are required and water quality variables are not required. An additional seepage rate variable may also be specified, and these details are listed in the `&outflow` section.

Several configuration variables and parameters must be provided:

- `num_outlet`: Number of streams to be simulated. Set to 0 if no streams are included.
- `flt_off_sw`: Names of the inflowing streams/rivers, separated by commas.
- `outl_elevs`: Steambed half-angle for each inflowing stream (Figure 4), separated by commas.
- `bsn_len_outl`: Steambed slope for each inflowing stream (Figure 4), separated by commas.
- `bsn_wid_outl`: Steambed drag for each inflowing stream (Table 1), separated by commas.
- `seepage_rate`: In addition to the above outflows, a constant seepage rate (Table 1), can be set.

Details of the inflow boundary condition data are summarised according to:

- `outflow_fl`: Name of the csv file containing the inflow data.
- `time_fmt`: Format of the time/data column in the inflow input file.
- `outflow_factor`: Scaling factor that is used to multiply the inflow data that is read in.

Table 5: Flow diagram showing the files required for operation of the model.

`outflow.csv` column	Units	Description
(1) TIME `time`	YYYY-MM-DD	Date
(2 … n_{OUT}+1) OUTFLOW `flow`	ML/day	Daily outflow rates of each outflow

Configuring the model to run water quality

In GLM v2 and above water quality can be simulated through coupling with FABM, or directly to the AED2 library (Hipsey, 2014). The water quality aspects of the simulation are engaged by including the `&wq_setup` information in `glm.nml`.

Several configuration variables and parameters must be provided:

- `wq_lib`: Name of the WQ library to be engaged: Either choose `'aed2'` or `'fabm'`.
- `ode_method`: Numerical method of solution of the biogeochemical model ODE equations.
- `split_factor`: Factor used for solution of the FABM biogeochemical ODEs.
- `bioshade_feedback`: Determines whether the extinction coefficient is updated based on WQ variables.
- `repair_state`: Determines whether small negative numbers in WQ variables should be zeroed.
- `multi_ben`: Flag to set WQ benthic fluxes to occur on all GLM layers, or just the bottom layer.
- `wq_nml_file`: Name of the input nml file to be read in for the WQ simulation.

Running the model

The model may be run by navigating to the directory where the `glm.nml` file is and executing the model executable `glm.exe`. The glm.exe file can be located in different directory and added to the system path if desired.

Windows users may wish to add the command into a `glm.bat`:

```
..\bin\glm.exe >glm.log
```

which will create a file that can simply be double-clicked from your file browser. The model will output to the NetCDF and/or csv files, which can then be plotted in a number of ways.

Note that the Windows pre-compiled model executable is distributed in a 32-bit and 64-bit release; choose an appropriate system.

Outputs and post-processing

The model includes several types of outputs, including the NetCDF file, an optional csv time-series file at a certain depth, and an optional live contour plot as the model simulation runs, to enable the modeller to monitor simulation progress.

Live output plotting: **plots.nml**

If the model is run with the optional command line argument "`--xdisp`" then the model simulation will display live plots of output parameters (Figure 8). The number of plots, parameters to plot and the colour bar limits are set in the file `plots.nml`, which may be simply configured according to the input variables shown below:

```
&plots
  nplots      = 4
  plot_width  = 400
  plot_height = 200
  title        = 'Temperature','Salinity','DO','extc'
  vars         = 'temp','salt','aed_oxygen_oxy',extc'
  min_z        =  0.0,   0.0,    0.0,   0.0
  max_z        = 30.0, 0.91, 400.0,   2.0
/
```

Table 6: Variables within the `output.nc` file available to be plot via `plots.nml`

Variable Name	Description	Units
`temp`	Temperature	°C
`salt`	Salinity	gL^{-1}
`rad`	Shortwave Radiation	Wm^{-2}
`extc`	Extinction Coefficient	m^{-1}
`dens`	Density	kgm^{-3}
`uorb`	Orbital Velocity (@ Sediment-Water Interface)	ms^{-1}
`taub`	Shear Stress (@ Sediment-Water Interface)	Nm^{-2}
`<WQ>`	Any water quality model variable, e.g. `aed_oxygen_oxy`. Refer to keywords used for AED in Hipsey (2014), or output summary information at the beginning of the simulation	various

Simulation summary: `lake.csv`

A daily summary of the simulation is summarised in the file `lake.csv`. This file includes *lake scale* information, related to surface heating and cooling, the lake water balance and other relevant metrics. For outputs of specific simulated variables at a particular depth, refer to the next sections.

Table 7: Summary information written to the `lake.csv` simulation output file.

Variable	Column	Description	Units	Note
date	A	Date	yyyy-mm-dd	
day	B	Julian day number	-	
Volume	C	Total lake volume	ML (1000 m^3)	
Tot Inflow Vol	D	Total daily inflow volume	ML	Sum of all inflow
Tot Outflow Vol	E	Total daily outflow volume	ML	Sum of all offtakes
Overflow Vol	F	Total daily volume of overflows	ML	Flows over the lake crest
Evaporation	G	Total daily volume of evaporation	ML	
Rain	H	Total daily volume of rainfall	ML	
Lake Level	I	Average lake level	m	
Surface Area	J	Lake surface area	m^2	
Blue Ice	K	Depth of blue ice	m	
Snow	L	Depth of snow	m	
White Ice	M	Depth of white ice	m	
Max Temp	N	Maximum daily temperature within lake	°C	
Min Temp	O	Minimum daily temperature within lake	°C	
Surface Temp	P	Surface temperature	°C	
Daily Qsw	Q	Daily heat input from shortwave radiation	MJ day^{-1}	
Daily Qe	R	Daily latent (evaporative) heat lost from the lake	MJ day^{-1}	
Daily Qh	S	Daily sensible heat flux	MJ day^{-1}	
Daily Qlw	T	Daily net longwave flux	MJ day^{-1}	
Light	U	Incident light intensity	μE m^{-2}	
Benthic Light	V	Percentage of the lake bottom exceeding $\phi_{BEN_{crit}}$	%	
T	W	Average wave period	s	
Hs	X	Average significant wave height	m	
L	Y	Average wave length of surface wind waves	m	
LakeNumber	Z	Lake number	-	
Max dT/dz	AA	Maximum recorded vertical temperature gradient	°C m^{-1}	

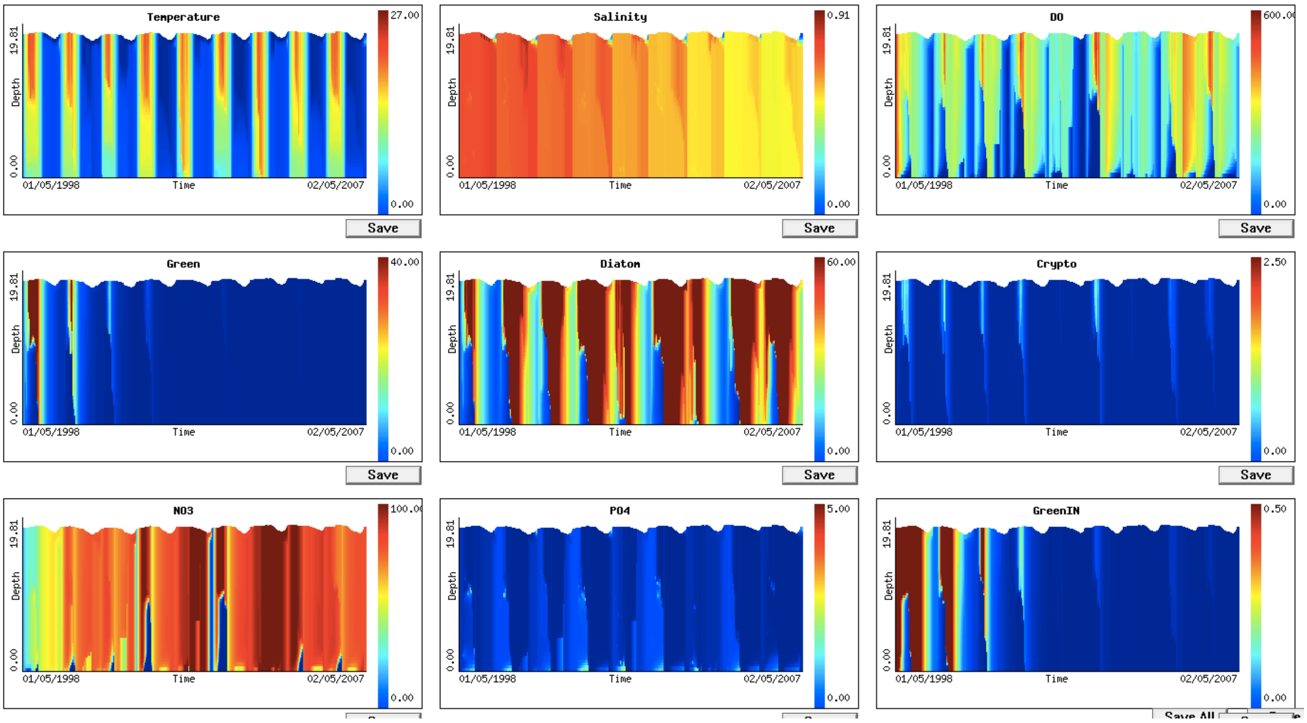

Figure 8: Example of live output plots generated via the libplot library provided with the model.

Plotting in EXCEL

For simple time-series plots, the user can configure outputs from the model directly to a csv file for a certain depth (defined relative to the bottom), and this information is defined in the `glm.nml &output` section. The columns to plot must also be listed in this section and are user-definable. Users can choose to output at any frequency.

Plotting in MATLAB

For more advanced or customised plots, then the user may load the `output.nc` NetCDF file into MATLAB. Recent versions of MATLAB (MATLAB 2011a or after) natively support NetCDF and can load the file directly. An example MATLAB script for plotting is shown below - this can be customised as required.

```
foldername = '../MyGLMSim/';
outname    = '../ MyGLMSim /figures /';
mkdir([outname]);

data         = nldncGLM([foldername,'/output.nc'])

varNames    = names_netcdf([foldername,'output.nc']);
varsToPlot = varNames([20:64]);

for ii = 1:length(varsToPlot)
    newFig  = plotGLM(varsToPlot{ii},data);

    figName = [outname,'/', varsToPlot {ii},'.png'];
    print(gcf,'-dpng', figName,'-opengl');
    close all
end
```

Plotting in R

The GLM output.nc NetCDF file can be read and plotted using the "R" package. A set of tools, "glmtools", has been developed in R by Jordan Read and Luke Winslow, and is available from: https://github.com/GLEON/glmtools. An example plot from R is below (Figure 9).

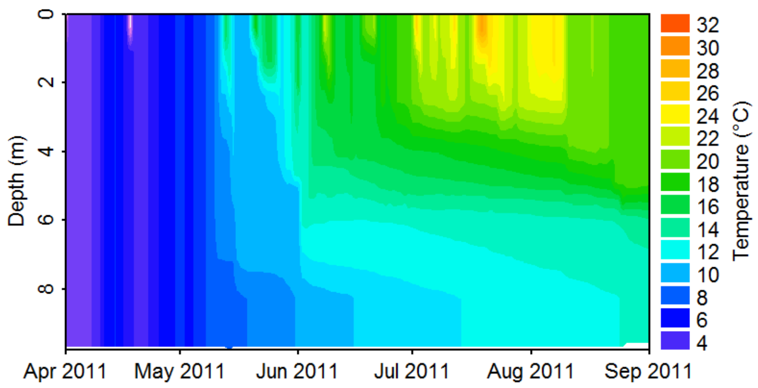

Figure 9: Image of temperature predicted by GLM, plotted using the R `glmtools` scripts.

Model Validation & Parameter Optimisation

There are numerous ways that model users may wish to assess model performance and adjust physical parameters in glm.nml to optimise their calibration with observed data. As part of a GLEON (gleon.org) lake modelling working group, a specific workflow for model assessment and parameter estimation has been trialled and is outlined below. The approach a) uses the GLEON "LakeAnalyzer" analysis scripts to assess model comparisons across a range of metrics, and b) combines these assessment scripts with a Markov Chain Monte Carlo (MCMC) method of parameter estimation.

Running the LakeAnalyzer validation

As part of a multi-lake comparison GLM has been compared against numerous different metrics of model performance. These include simple measures like surface or bottom temperature, however it is also possible to compare the model's performance in capturing higher-order metrics relevant to physical limnology. To calculate these on the model and field data, the LakeAnalyzer routines provided by Read *et al.* (2012). These have been adapted for GLM use and can be called via the run using the `calcGLMModelFit.m` and `plotGLMModelFit.m` scripts. An example output from Lake Kinneret is shown in Figure 10.

Field Files: `model_fld_temp.wtr` & `model.bth`

Together the `model_fld_temp.wtr` and the `model.bth` files give observed water temperature data and lake shape details that are compared against the model output. Both files are comma separated text files in the same format as required for running LakeAnalyzer.

The `model_fld_temp.wtr` file is a simple file consisting of time-stamped thermistor chain data. The first row given the date and thermistor chain ID's (Figure 11a). Note the date format must be saved as YYYY-MM-DD, prior to saving as a csv file.

The `model.bth` file is a simple two column file consisting of each thermistors depth, and the area of the bathymetry at that depth (Figure 11b). Save the files as a csv.

Running the MCMC parameter estimation

As part of the modelling process, users may desire to adjust the GLM physical parameters to get the best fit with available field data. GLM may be run with a Markov Chain Monte Carlo (MCMC) routine that can be used to provide improved parameter estimates. On the GLM website we provide a version of GLM that works with the MCMC code provided by Haario *et al.* (2006), though users may wish to develop their own optimisation approach.

The MCMC routines are available as MATLAB scripts that will call `glm.exe` during the run. This is run using the `runMCMC.m` script. We have also prepared a pre-compiled form of the procedure that can run on Windows via the command prompt, independent of MATLAB being installed, by running `runMCMC.exe`. Note that for the pre-compiled version that has been supplied, users must have the MATLAB runtime environment (MCR) installed (http://www.mathworks.com.au/products/compiler/mcr/).

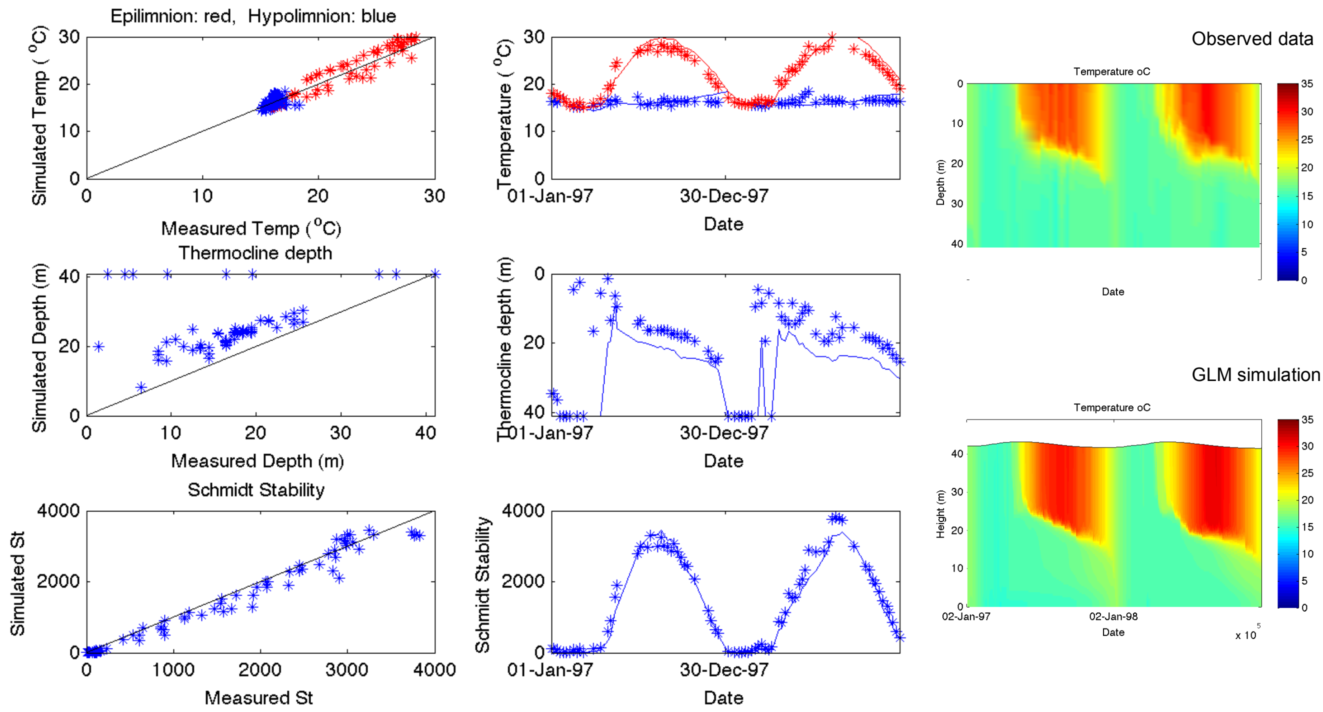

Figure 10: Example output from the GLM model assessment scripts.

Thermistor Chain ID's

Date Time (ISO Format)

	A	B	C	D	E	F	G
1	DataTime	temp0	temp0.5	temp1.0	temp1.5	temp2.0	temp2.5
2	1997/01/01 00:00	18.014375	18.0141875	18.014	18.00883333	18.00366667	18.00164583
3	1997/01/05 00:00	18.014375	18.0141875	18.014	18.00883333	18.00366667	18.00164583
4	1997/01/14 00:00	17.8175	17.80947222	17.80144444	17.79955556	17.79766667	17.79033333
5	1997/01/19 00:00	17.36322785	17.36197756	17.36072727	17.34280114	17.324875	17.3104375
6	1997/01/26 00:00	16.94884375	16.95194568	16.95504762	16.95589881	16.95675	16.95598611
7	1997/02/02 00:00	16.19581481	16.19803241	16.20025	16.20218056	16.20411111	16.20318056
8	1997/02/09 00:00	15.3412	15.34665556	15.35211111	15.35186806	15.351625	15.35142361
9	1997/02/16 00:00	15.95333333	15.92305556	15.89277778	15.867	15.84122222	15.83379861
10	1997/02/24 00:00	15.16827273	15.16909091	15.16990909	15.16889205	15.167875	15.16438194
11	1997/03/02 00:00	16.247	16.25240909	16.25781818	16.18484659	16.111875	15.85782639
12	1997/03/09 00:00	15.22820588	15.20935294	15.1905	15.1785	15.1665	15.1604375
13	1997/03/30 00:00	15.99888889	15.99727778	15.99566667	15.99138889	15.98711111	15.98499306
14	1997/04/13 00:00	16.949	16.9379375	16.926875	16.90325	16.879625	16.848
15	1997/04/29 00:00	19	19	19	18.5	18	18
16	1997/05/04 00:00	19.8	19.8	19.8	19.8	19.8	19.8
17	1997/05/13 00:00	23.90209859	23.9003618	23.898625	23.89447917	23.89033333	23.87566667
18	1997/05/18 00:00	24.57325	24.5649375	24.556625	24.54453472	24.53244444	24.52807222
19	1997/06/29 00:00	27.4	27.4	27.4	27.35	27.3	27.05
20	1997/07/06 00:00	27.5	27.5	27.5	27.5	27.5	27.5
21	1997/07/20 00:00	27.2	27.2	27.2	27.2	27.2	27.2

Each Thermistor in the wtr must be represented by a depth

Bathymetry Depths	Bathymetry Areas
0	170000
1	167000
4	162000
5	161000
6	160000
7	158000
8	157000
9	155000
10	153000
11	151000
12	150000
13	148000
14	146000
15	143000
16	139000
17	136000
18	132000
19	128000
20	123000
21	118000
22	113000
23	107000
24	102000
25	96400
26	90975

Figure 11: Outline of the required field data files to run the model validation for a) model_fld_tmp.wtr and b) model.bth.

To run the model as part of the MCMC routine, users must prepare several extra files and directories. These include files for providing the observed field data (as above) and also files associated with the MCMC routine:

- Field/model.bth
- Field/model_fld_temp.wtr
- InputFiles/glm_init.nml
- InputFiles/mcmc_config.nml

The model will run and output a log of model RMSE and other information about the performance of different parameter combinations. These will be written to files in the `Results/` folder.

MCMC files: `glm_init.nml` & `mcmc_config.nml`

The `InputFiles/glm_init.nml` file is simply a duplicate of the starting simulation GLM nml file. The structure of this file is described in the above sections.

The `InputFiles/mcmc_config.nml` file is a namelist file which specifies certain parameters which governs how the optimisation routine functions. Currently, there are four sections:

- `&config`
- `&dataset`
- `&ssh`
- `&params`

The `&config` section contains the following variables:

- *Fld_temp_file* – Path to model_fld_temp.wtr file
- *Varname* – GLM variable name of data within the wtr file (e.g. 'temp')
- *Remote* – Switch for whether routine is run locally (0) or an a server via ssh (1)
- *Nsim_ini* – Number of simulations to run to get base values
- *Nsim_full* – Number of optimisation simulations to run.

The `&dataset` section contains the following variables:

- *Data_Subsets*
- *Model_Fit* – Type of error calculation (e.g., RMSE, Nash-Sutcliffe, R^2, etc)

The `&ssh` section contains the following variables:

- *Host_Name*
- *Usr_Name*
- *Password*
- *Remote_Dir*
- *Run_GLM*
- *Output_File*
- *Varname*

The `&params` section contains the following variables and these are those that are to be included in the parameter optimisation. The values assigned to these variables is the starting parameter vector (see also Table 1):

- *coef_mix_conv* – Coefficient related to mixing efficiency of convective overturn.
- *coef_wind_shear* – Coefficient related to mixing efficiency of wind shear events.
- *coef_mix_turb* – Coefficient related to mixing efficiency of unsteady turbulence.
- *coef_mix_kh* – Coefficient related to Kelvin Helmholtz turbulent billows.
- *coef_mix_hyp* – Coefficient related to mixing efficiency of hypolimnetic turbulence
- *ce* – Bulk transfer coefficient for latent heat, C_E.
- *ch* – Bulk transfer coefficient for sensible heat, C_H.
- *cd* – Bulk transfer coefficient for momentum, C_D.

Examples & Support

Downloads & Further Support

To download the model, visit: http://aed.see.uwa.edu.au/research/models/GLM/

Support and FAQ's are available at the Aquatic Ecosystem Modelling Network (AEMON) website:

http://sites.google.com/site/aquaticmodelling/

For specific development requests, please contact Dr Louise Bruce or A/Prof Matthew Hipsey from the School of Earth and Environment, The University of Western Australia.

louise.bruce@uwa.edu.au
matt.hipsey@uwa.edu.au

Example Applications

Numerous applications are presented online as part of the GLM Multi-Lake Comparison Project (MLCP):

http://aed.see.uwa.edu.au/research/models/GLM/Pages/projects.html

Two example setups - "*warmlake*" and "*coldlake*" - are also available for download. These simulations demonstrate working setups configured using various simulation options, including ice-cover for coldlake.

References

Ashton, G.D. (ed.), 1986. River and lake ice engineering. Water Resources Publication.

Babanin, A.V. and Makin, V.K., 2008. Effects of wind trend and gustiness on the sea drag: Lake George study. *Journal of Geophysical Research: Oceans*, 113(C2).

Bird, R.E., 1984. A simple, solar spectral model for direct-normal and diffuse horizontal irradiance. *Solar energy*, 32: 461-471.

Businger, J.A., Wyngaard, J.C., Izumi, Y., Bradley, E.F., 1971. Flux profile relationships in the atmospheric surface layer. *Journal of Atmospheric Sciences*, 28: 181-189.

Condie, S.A. and Webster, I.T. 1997. The influence of wind-stress, temperature, and humidity gradients on evaporation from reservoirs. *Water Resources Research*, 33: 2813-2822.

Dyer, A.J., 1974. A review of flux-profile relationships. *Boundary-Layer Meteorology*, *7*: 363-372.

Fischer, H.B., List, E.G., Koh, R.C.Y., Imberger, J. and Brooks, N.H., 1979. Mixing in Inland and Coastal Waters. Academic Press.

Fischer et al., 1980. Chapter 6: Mixing in Reservoirs.

Francey, R.J., & Garratt, J.R., 1978. Eddy flux measurements over the ocean and related transfer coefficients. *Boundary-Layer Meteorology*, 14: 153-166.

Gal, G., Imberger, J., Zohary, T., Antenucci, J., Anis, A., & Rosenberg, T., 2003. Simulating the thermal dynamics of Lake Kinneret. *Ecological Modelling*, 162: 69-86.

Gill, A.E., 1982. Atmosphere-ocean dynamics (Vol. 30). Academic press.

Gu, R., and Stefan, H.G., 1993. Validation of cold climate lake temperature simulation. *Cold regions science and technology*, 22: 99-104.

Haario, H., Laine, M., Mira, A. and Saksman, E., 2006. DRAM: Efficient adaptive MCMC, *Statistics and Computing* 16: 339-354.

Hamilton, D.P. & Schladow, S.G. 1997. Water quality in lakes and reservoirs. Part I Model description. *Ecological Modelling*, 96: 91–110.

Harvey, L.D.D., 1990. Testing alternative parameterizations of lateral melting and upward basal heat flux in a thermodynamic sea ice model, *Journal of Geophysical Research,* 95: 7359-7365.

Hicks, B.B. 1975. A procedure for the formulation of bulk transfer coefficients over water. *Boundary Layer Meteorology*, 8: 315-324.

Hicks, B.B., 1972. Some evaluations of drag and bulk transfer coefficients over water. *Boundary Layer Meteorology*, 3: 201:213.

Hipsey, M.R. and Sivapalan, M. 2003. Parameterizing the effect of a wind-shelter on evaporation from small waterbodies. *Water Resources Research*, 39: 1339.

Hipsey, M.R., (ed.), 2014. Modelling aquatic dynamics with the AED modelling library. AED Report #30, The University of Western Australia, Perth, Australia.

Hocking, G.C., and Patterson, J.C., 1991. Quasi-two-dimensional reservoir simulation model. *Journal of Environmental Engineering*, 117: 595-613.

Idso, S.B., and Jackson, R.D., 1969. Thermal radiation from the atmosphere. *Journal of Geophysical Research*, 74: 5397-5403.

Imberger , J., Patterson, J., Hebbert, B. and Loh, I.,1978. Dynamics of reservoir of medium size. *Journal of the Hydraulics Division - ASCE*, 104 No HY5: 725-743.

Imberger, J. and Patterson, J.C., 1981. *A dynamic reservoir simulation model-DYRESM:5*. In: H.B. Fisher (ed.), Transport Models for Inland and Coastal Waters. Academic Press, New York: 310-361.

Imberger, J., and Patterson, J.C., 1990. *Physical Limnology*, p. 303-475. In: T. Wu (ed.), Advances in applied mechanics 27. Academic.

Imboden, D.M. and Wüest, A., 1995. *Mixing Mechanisms in Lakes*, p. 83-138. In: A. Lerman, D.M. Imboden and J.R. Gat (eds.), Physics and Chemistry of Lakes. Springer-Verlag.

Jellison, R. and Melack, J.M. 1993. Meromixis and vertical diffusivities in hypersaline Mono Lake, California. *Limnology and Oceanography*, 38: 1008–1019.

Ji, Z.G., 2008. Hydrodynamics and water quality: modeling rivers, lakes, and estuaries. John Wiley & Sons.

Kim, J-W., 1976. A generalized bulk model of the oceanic mixed layer. *Journal of Physical Oceanography*, 6: 686-695.

Kirk, J.T.O., 1994. Light and photosynthesis in aquatic ecosystems. Cambridge University Press.

Kleinhans, M.G. and Grasmeijer, B.T., 2006. Bed load transport on the shoreface by currents and waves. *Coastal Engineering*, 53 : 983-996.

Kraus, E.B. and Turner, J.S., 1967. A one-dimensional model of the seasonal thermocline: II The general theory and its consequences. *Tellus*, 19: 98-106.

Laenen A. and LeTourneau A.P. 1996. Upper Klamath Lake nutrient loading study – Estimate of wind-induced resuspension of bed sediment during periods of low lake elevation. *US Geological Survey Open-File Report 95-414*, 11 pp

Launiainen, J., 1995. Derivation of the relationship between the Obukhov stability parameter and the bulk Richardson number for flux-profile studies. *Boundary Layer Meteorology*, 76: 165-179.

Launiainen, J., and Cheng, B. 1998. Modelling of ice thermodynamics in natural water bodies. *Cold Region Science and Technology*, 27: 153-178.

Launiainen, J., and Vihma, T., 1990. Derivation of turbulent surface fluxes—An iterative flux-profile method allowing arbitrary observing heights. *Environmental Software*, 5: 113-124.

Le Roux, J.P., 2007. A simple method to determine breaker height and depth for different deepwater wave height/length ratios and sea floor slopes. *Coastal Engineering*, 54 : 271-277.

Luo, L., Hamilton, D., and Han, B., 2010. Estimation of total cloud cover from solar radiation observations at Lake Rotorua, New Zealand. *Solar Energy*, 84: 501-506.

McKay, G.A., 1968. Problems of measuring and evaluating snow cover. In: *Proceedings Workshop Seminar of Snow Hydrology.(Secretariat Canadian National Committee for the IHD*, Ottawa: 49-62.

McCord, S.A., and Schladow, S.G., 1998. Numerical simulations of degassing scenarios for CO2-rich Lake Nyos, Cameroon. *Journal of Geophysical Research: Solid Earth*, 103(B6): 12355-12364.

Mooij, W.M., Trolle, D., Jeppesen, E., Arhonditsis, G., Belolipetsky, P.V., Chitamwebwa, D.B.R., Degermendzhy, A.G., DeAngelis, D.L., De Senerpont Domis, L.N., Downing, A.S., Elliott, A.E., Fragoso Jr, C.R., Gaedke, U., Genova, S.N., Gulati, R.D., Håkanson, L., Hamilton, D.P., Hipsey, M.R., Hoen, J., Hülsmann, S., Los, F.J., Makler-Pick, V., Petzoldt, T., Prokopkin, I.G., Rinke, K., Schep, S.A., Tominaga, K., Van Dam, A.A., Van Nes, E.H., Wells, S.A., Janse, J.H., 2010. Challenges and opportunities for integrating lake ecosystem modelling approaches. *Aquatic Ecology*, 44: 633–667.

Monin, A.S., and Obukhov, A.M., 1954. Basic laws of turbulent mixing in the atmosphere near the ground. *Jr. Akad. Nauk SSSR Geofiz. Inst.*, 24: 163-187.

Patterson, J.C., Hamblin, P.F., and Imberger, J. 1984. Classification and dynamics simulation of the vertical density structure of lakes. *Limnology and Oceanography*, 29: 845-861.

Patterson, J.C., and Hamblin, P.F., 1988. Thermal simulation of a lake with winter ice cover. *Limnology and Oceanography*, 33: 323-338.

Paulson, C. A., 1970. The mathematical representation of wind speed and temperature profiles in the unstable atmospheric surface layer. *Journal of Applied Meteorology*, 9: 857-861.

Read, J.S., Hamilton, D.P., Jones, I.D., Muraoka, K., Winslow, L.A., Kroiss, R., Wu, C.H. and Gaiser, E., 2011. Derivation of lake mixing and stratification indices from high-resolution lake buoy data. *Environmental Modelling and Software,* 26: 1325–1336.

Read, J., Hansen, G., Van Den Hoek, J., Hanson, P., Bruce, L.C., Markfort, C.D., 2014. Simulating 2368 temperate lakes reveals weak coherence in stratification phenology. *Ecological Modelling*, 291: 142-150.

Rogers, C.K., Lawrence, G.A., and Hamblin, P.F., 1995. Observations and numerical simulation of a shallow ice-covered mid-latitude lake. *Limnology and Oceanography*, 40: 374-385.

Sherman, F.S., Imberger, J. and Corcos, G.M., 1978. Turbulence and mixing in stably stratified waters. *Ann. Rev. Fluid Mech.* 10: 267-288.

Spigel, B., 1978. Wind mixing in Lakes. PhD thesis., University of California, Berkeley.

Spigel, R.H., Imberger, J. Rayner, K.N., 1986. Modeling the diurnal mixed layer. *Limnology and Oceanography*, 31: 533-556.

Strub, P.T. and Powell, T.M., 1987. Surface temperature and transport in Lake Tahoe: inferences from satellite (AVHRR) imagery. *Continental Shelf Research*, 7: 1001-1013.

Swinbank, W.C. 1963. Longwave radiation from clear skies. *Quarterly Journal of the Royal Meteorological Society*, 89: 339-348.

Tennessee Valley Authority, 1972. Heat and mass transfer between a water surface and the atmosphere. Water Resources Research Laboratory Report 14, Report No. 0-6803.

Tabata, S., 1973. A simple but accurate formula for the saturation vapour pressure over liquid water. *Journal of Applied Meteorology*, 12: 1410-1411.

Trolle, D., Hamilton, D.P., Hipsey, M.R., Bolding, K., Bruggeman, J., Mooij, W. M., Janse, J. H., Nielsen, A., Jeppesen, E., Elliott, J.E., Makler-Pick, V., Petzoldt, T., Rinke, K., Flindt, M. R., Arhonditsis, G.B., Gal, G., Bjerring, R., Tominaga, K., Hoen, J., Downing, A.S., Marques, D. M., Fragoso Jr, C.R., Søndergaard, M. and Hanson, P.C., 2012. A community-based framework for aquatic ecosystem models. *Hydrobiologia*, 683: 25-34.

UNESCO. 1981. Technical papers in Marine Science. No. 36.

Vavrus, S.J., Wynne, R.H., and Foley, J.A., 1996. Measuring the sensitivity of southern Wisconsin lake ice to climate variations and lake depth using a numerical model. *Limnology and Oceanography*, 41: 822-831.

Vickers, D., Mahrt, L., and Andreas, E.L., 2013. Estimates of the 10-m neutral sea surface drag coefficient from aircraft eddy-covariance measurements. *Journal of Physical Oceanography*, 43: 301-310.

Weinstock, J., 1981. Vertical turbulence diffusivity for weak or strong stable stratification. *Journal of Geophysical Research*, 86(C10): 9925-9928.

Wu J., 1973. Wind induced entrainment across a stable density interface. *Journal of Fluid Mechanics*, 61: 275-278.

Xenopoulos, M.A. and Schindler, D.W., 2001. The environmental control of near-surface thermoclines in boreal lakes. *Ecosystems*, 4: 699-707.

Yajima, H. and Yamamoto, S., 2014. Improvements of radiation estimations for a simulation of water temperature in a reservoir. *Annual Journal of Hydraulic Engineering*, JSCE, 59, submitted.

Yao, H., Samal, N.R., Joehnk, K.D., Fang, X., Bruce, L.C., Pierson, D.C., Rusak, J.A. and James, A., 2014. Comparing ice and temperature simulations by four dynamic lake models in Harp Lake: past performance and future predictions. *Hydrological Processes*, 28: 4587–4601.

Yeates, P.S. and Imberger, J. 2004. Pseudo two-dimensional simulations of internal and boundary fluxes In stratified lakes and reservoirs. *International Journal of River Basin Research,* 1: 1-23.

Appendices

A: Bird solar radiation model

The Bird Clear Sky Model (BCSM) was developed by (Bird, 1984). This model predicts clear-sky direct beam, hemispherical diffuse, and total hemispherical broadband solar radiation on a horizontal surface. Average solar radiation is computed hourly with 10 user-specified input parameters (Table A1). The default parameters used in GLM are as outlined in this table, but may be customised using the `&bird` parameter block in `glm.nml`.

Table A1: Parameters required for the BCSM model.

Variable	Description	Value used to fit to data from Perth, WA	Value used in Luo et al. (2010) for Hamilton, NZ
Lat	Latitude (+ for N)	-31.77	
Long	Longitude (+ for E)	116.03	
TZ	Time Zone indicated by number of hours from GMT	+7.5	
AP	Atmospheric Pressure (millibars)	1013	
Oz	Ozone Conc. (atm-cm)	0.279	0.279 - 0.324
W	Total Precipitable Water Vapour (atm-cm)	1.5	1.1 - 2.2
AOD_{500}	Aerosol Optical Depth at 500 nm	0.1	0.033 - 0.017
AOD_{380}	Aerosol Optical Depth at 380 nm	0.15	0.038 - 0.019
α_{SW}	Surface albedo	0.2	0.2

The solar constant in the model is taken as 1367 W/m^2. This is corrected due to the elliptical nature of the earth's orbit and consequent change in distance to the sun. This calculation gives us the Extra-Terrestrial Radiation ($\hat{\phi}_{ETR}$), at the top of the atmosphere:

$$\hat{\phi}_{ETR} = 1367\left(1.00011 + 0.034221\cos(\Phi_{day}) + 0.00128\sin(\Phi_{day}) + 0.000719\cos(\Phi_{day})\right) \tag{A1}$$

where the day angle, Φ_{day}, is computed using, d, the day number:

$$\Phi_{day} = 2\pi\left(\frac{d-1}{365}\right) \tag{A2}$$

The solar declination, Φ_{dec} (radians), is computed from:

$$\Phi_{dec} = \begin{bmatrix} 0.006918 - 0.399912\,cos(\Phi_{day}) + 0.070257\,sin(\Phi_{day}) - 0.006758\,cos\left(2(\Phi_{day})\right) + \\ 0.000907\,sin(2\Phi_{day}) - 0.002697\,cos\left(3(\Phi_{day})\right) + 0.00148\,sin\left(3(\Phi_{day})\right) \end{bmatrix} \tag{A3}$$

We then solve the equation of time:

$$EQT = \begin{bmatrix} 0.0000075 + 0.001868\,cos(\Phi_{day}) - 0.032077\,sin(\Phi_{day}) \\ -0.014615\,cos\left(2(\Phi_{day})\right) - 0.040849\,sin\left(2(\Phi_{day})\right) \end{bmatrix} \times 229.18 \tag{A4}$$

in order to compute the hour angle, Φ_{hr}, calculated with noon zero and morning positive as:

$$\Phi_{hr} = 15(hr - 12.5) + Long - 15\,TZ + \left(\frac{EQT}{4}\right) \tag{A5}$$

where TZ is the time-zone shift from GMT. The zenith angle, Φ_{zen} (radians), is calculated from:

$$\cos(\Phi_{zen}) = \cos(\Phi_{dec})\cos(\Phi_{hr})\cos(Lat) + \sin(\Phi_{dec})\sin(Lat) \tag{A6}$$

When Φ_{zen} is less than 90°, the air mass factor is calculated as:

$$\text{AM} = \left[cos(\Phi_{zen}) + \frac{0.15}{(93.885 - \Phi_{zen})^{1.25}}\right]^{-1} \tag{A7}$$

which is corrected for atmospheric pressure, p (hPa),

$$AM_p = \frac{AM\, p}{1013} \tag{A8}$$

AM_P is then used to calculate the Rayleigh Scattering as:

$$T_{rayleigh} = e^{[(-0.0903\, AM_p{}^{0.84})+(1+AM_p - AM_p{}^{1.01})]} \tag{A9}$$

The effect of ozone scattering is calculated by computing ozone mass, which for positive air mass is:

$$T_{ozone} = \left[1 - \left(0.1611\,(Oz\,AM)\,\left(1 + 139.48\,(Oz\,AM)\right)^{-0.3035}\right) - \frac{0.002715\,(Oz\,AM)}{1 + 0.044\,(Oz\,AM) + 0.0003\,(Oz\,AM)^2}\right] \tag{A10}$$

The scattering due to mixed gases for positive air mass is calculated as:

$$T_{mix} = e^{\left[-0.0127\, AMp^{0.26}\right]} \tag{A11}$$

Then the water scattering is calculated by getting the water mass:

$$Wm = WAM_p \tag{A12}$$

where W is the precipitable water vapour. This can be approximated from dew point temperature, eg.:

$$\ln W = a\, T_d + b \tag{A13}$$

where a and b are regression coefficients which have been taken as 0.09, 0.07, 0.07 and 0.08 for values of a while b is 1.88, 2.11, 2.12 and 2.01 in spring, summer, autumn and winter (Luo et al., 2010).

Then the water scattering effect is calculated as:

$$T_{water} = \left[1 - \frac{(2.4959\, Wm)}{1 + (79.034\, Wm)^{0.6828} + 6.385\, Wm}\right] \tag{A14}$$

The scattering due to aerosols requires the Aerosol Optical Depth at 380 nm and 500 nm:

$$TauA = 0.2758\, AOD_{380} + 0.35\, AOD_{500} \tag{A15}$$

and the scattering due to aerosols is then calculated as:

$$T_{aerosol} = e^{(-TauA)^{0.873}\left(1+TauA-TauA^{0.7088}\right) AM^{0.9108}} \tag{A16}$$

We also define:

$$T_{aa} = 1 - [0.1\,(1 - AM + AM^{1.06})\,(1 - T_{aerosol})] \tag{A17}$$

and:

$$\frac{0.5(1 - T_{rayleigh}) + 0.84(1 - T_{as})}{1 - AM + AM^{1.02}} \tag{A18}$$

where the 0.84 value used is actually the proportion of scattered radiation reflected in the same direction as incoming radiation.

The direct beam radiation on a horizontal surface at ground level on a clear day is given by,

$$\hat{\phi}_{DB} = 0.9662\,\hat{\phi}_{ETR}\, T_{rayleigh}\, T_{ozone}\, T_{mix}\, T_{watvap}\, T_{aerosol}\; cos(\Phi_{zen}) \tag{A19}$$

$$\hat{\phi}_{AS} = 0.79\,\hat{\phi}_{ETR}\; T_{ozone} T_{mix}\, T_{watvap}\, T_{aa}\; cos(\Phi_{zen}) \tag{A20}$$

The total irradiance hitting the surface is therefore (W m^{-2}):

$$\hat{\phi}_{SW} = \frac{\hat{\phi}_{DB} + \hat{\phi}_{AS}}{1 - (\alpha_{SW}\,\alpha_{SKY})} \tag{A21}$$

The albedo is computed for the sky as:

$$\alpha_{SKY} = 0.068 + (1 - 0.84)\left(1 - \frac{T_{aerosol}}{T_{aa}}\right) \tag{A22}$$

B: Non-neutral bulk transfer coefficients

The iterative procedure used in this analysis is conceptually similar to the methodology discussed in detail in Launiainen and Vihma (1990). The first estimate for the neutral drag coefficient is specified as a function of windspeed as it is has been commonly observed that C_{DN} increases with U_{10} (Figure A1). This is modelled by first by estimating:

$$C_{DN-10} = \begin{cases} 0.001 & U_{10} \le 5 \\ 0.001\,(1 + 0.07[U_{10} - 5]) & U_{10} > 5 \end{cases} \quad \text{Option 1 : Francey and Garratt (1978), Hicks (1972)} \tag{A23}$$

$$C_{DN-10} = 1.92 \times 10^{-7} U_{10}^3 + 0.00096 \quad \text{Option 2 : Babanin and Makin (2008)}$$

and then computing the Charnock formula with the smooth flow transition (e.g., Vickers et al., 2013):

$$z_o = \frac{\alpha u_*^2}{g} + 0.11 \frac{\nu}{u_*} \tag{A24}$$

where α is the Charnock constant (0.012), u_* is the friction velocity ($\sqrt{C_{DN-10}\, U_{10}^2}$) using Eq A23, and the final drag is re-computed using:

$$C_{DN-10} = \left[\frac{k}{\ln\left(\frac{10}{z_o}\right)} \right]^2 \tag{A25}$$

where k is the von Karman constant. Note the neutral humidity/temperature coefficient, C_{HWN-10}, is held constant at the user defined C_H value and doesn't scale with windspeed.

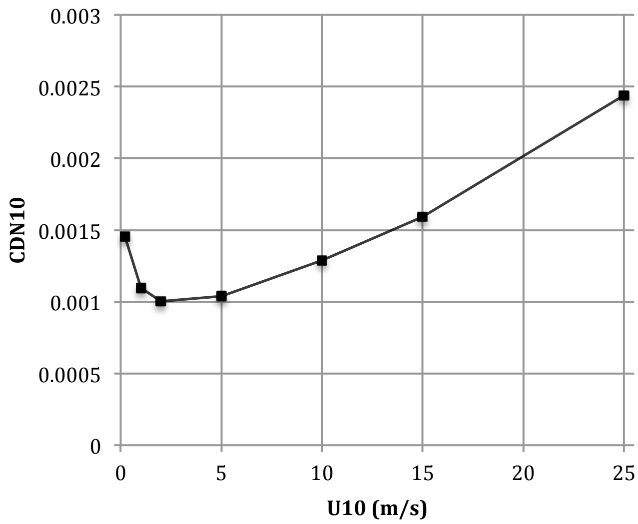

Figure A1: Scaling of the 10m neutral drag coefficient with wind speed (Eqs. A23-25)

Under non-neutral conditions in the atmospheric boundary layer, the transfer coefficients vary due to stratification seen in the air column, as was parameterised by Monin and Obukhov (1954) using the now well-known stability parameter, *z/L*, where *L* is the Obukhov length defined as:

$$L = \frac{-\rho_a u_*^3 \theta_V}{kg\left(\frac{H}{c_p} + 0.61 \frac{\theta E}{\lambda}\right)} \tag{A26}$$

where $\theta_V = \theta(1 + 0.61q)$ is the virtual temperature and H and E are the bulk fluxes. Paulson (1970) presented a solution for the vertical profiles of wind speed, temperature and moisture in the developing boundary layer as a function of the Monin-Obukhov stability parameter; the so-called flux-profile relationships:

$$U_z = \frac{u_*}{k}\left[\ln\left(\frac{z}{z_o}\right) - \psi_M\left(\frac{z}{L}\right)\right] \tag{A27a}$$

$$\theta_z - \theta_s = \frac{\theta_*}{k}\left[\ln\left(\frac{z}{z_\theta}\right) - \psi_H\left(\frac{z}{L}\right)\right] \tag{A27b}$$

$$q_z - q_s = \frac{q_*}{k}\left[\ln\left(\frac{z}{z_q}\right) - \psi_E\left(\frac{z}{L}\right)\right] \tag{A27c}$$

where ψ_M, ψ_H and ψ_E are the similarity functions for momentum, heat and moisture respectively, and z_o, z_θ and z_q are their respective roughness lengths. For unstable conditions ($L<0$), the stability functions are defined as (Paulson 1970; Businger *et al.*, 1971; Dyer, 1974):

$$\psi_M = 2\ln\left(\frac{1+x}{2}\right) + \ln\left(\frac{1+x^2}{2}\right) - 2\tan^{-1}x + \frac{\pi}{2} \tag{A28a}$$

$$\psi_E = \psi_H = 2\ln\left(\frac{1+x^2}{2}\right) \tag{A28b}$$

where

$$x = \left[1 - 16\left(\frac{z}{L}\right)^{1/4}\right] \tag{A29}$$

During stable stratification ($L>0$) they take the form:

$$\psi_M = \psi_E = \psi_H = \begin{cases} -5\left(\frac{z}{L}\right) & 0 < \frac{z}{L} < 0.5 \\ 0.5\left(\frac{z}{L}\right)^{-2} - 4.25\left(\frac{z}{L}\right)^{-1} - 7\left(\frac{z}{L}\right) \quad - 0.852 & 0.5 < \frac{z}{L} < 10 \\ \ln\left(\frac{z}{L}\right) - 0.76\left(\frac{z}{L}\right) - 12.093 & \frac{z}{L} > 10 \end{cases} \tag{A30}$$

Substituting equations (17)-(18) into (A27) and ignoring the similarity functions leaves us with neutral transfer coefficients as a function of the roughness lengths:

$$C_{XN} = k^2\left[\ln\left(\frac{z}{z_o}\right)\right]^{-1}\left[\ln\left(\frac{z}{z_X}\right)\right]^{-1} \tag{A31}$$

where N denotes the neutral value and X signifies either D, H or E for the transfer coefficient and o, θ or q for the roughness length scale. Inclusion of the stability functions into the substitution and some manipulation (Imberger and Patterson, 1990; Launianen and Vihma, 1990) yields the transfer coefficients relative to these neutral values:

$$\frac{C_X}{C_{XN}} = \left[1 + \frac{C_{XN}}{k^2}\left(\psi_M\psi_X - \frac{k\psi_X}{\sqrt{C_{DN}}} - \frac{k\psi_M\sqrt{C_{DN}}}{C_{XN}}\right)\right] \tag{A32}$$

Hicks (1975) and Launianen and Vihma (1990) suggested an iterative procedure to solve for the stability corrected transfer coefficient using (A32) based on some initial estimate of the neutral value. The surface flux is subsequently estimated according to (17-18) and used to provide an initial estimate for L (equation A26). The partially corrected transfer coefficient is then recalculated and so the cycle goes. Strub and Powell (1987) and Launiainen (1995), presented an alternative based on estimation of the bulk Richardson number, Ri_B, defined as:

$$Ri_B = \frac{gz}{\theta_V}\left(\frac{\Delta\theta + 0.61\,\theta_V\Delta q}{U_z^2}\right) \tag{A33}$$

and related as a function of the stability parameter, z/L, according to:

$$Ri_B = \frac{z}{L}\left(\frac{k\sqrt{C_{DN}}/C_{HWN} - \psi_{HW}}{\left[k/\sqrt{C_{DN}} - \psi_M\right]^2}\right) \tag{A34}$$

where it is specified that $C_{HN} = C_{WN} = C_{HWN}$. Figure A2 illustrates the relationship between the degree of atmospheric stratification (as described by both the bulk Richardson number and the Monin-Obukhov stability parameter) and the transfer coefficients scaled by their neutral value.

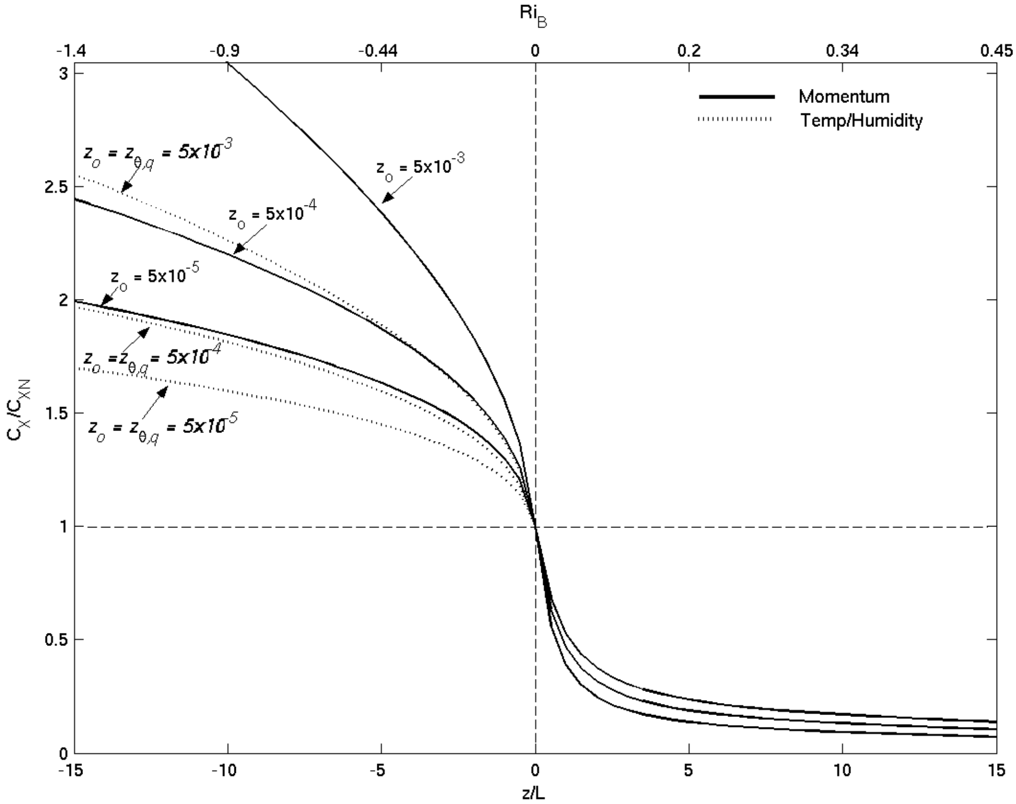

Figure A2: Relationship between atmospheric stability (bottom axis – *z/L*, top axis – Ri_B) and the bulk-transfer coefficients relative to their neutral value (C_X/C_{XN} where *X* represents *D*, *H* or *W*) for several roughness values (computed from Eq. A32). The solid line indicates the momentum coefficient variation (C_D/C_{DN}) and the broken line indicates humidity and temperature coefficient (C_{HW}/C_{HWN}) variation.